Polymer Testing 130 (2024) 108293

Contents lists available at ScienceDirect

Polymer Testing

journal homepage: www.elsevier.com/locate/polytest

Unlocking superior properties in polypropylene/polyethylene terephthalate (PP/PET) blends using an ethylene-butylene-acrylate terpolymer reactive compatibilizer

Sebastián Coba-Daza [a,e], Itziar Otaegi [a], Nora Aramburu [a], Gonzalo Guerrica-Echevarria [a], Lourdes Irusta [a], Alba González [a], Lena Neubauer [c], Georg Ramer [c], Bernhard Lendl [c], Gerhard Hubner [e], Dario Cavallo [d,**], Davide Tranchida [e,***], Alejandro J. Müller [a,b,*]

[a] POLYMAT and Department of Advanced Polymers and Materials: Physics, Chemistry and Technology, Faculty of Chemistry, University of the Basque Country UPV/EHU, Paseo Manuel de Lardizabal 3, 20018, Donostia-San Sebastián, Spain
[b] IKERBASQUE, Basque Foundation for Science, Bilbao, 48013, Spain
[c] Institute of Chemical Technologies and Analytics, TU Wien, Getreidemarkt 9/E164-02-1, Vienna, 1060, Austria
[d] Department of Chemistry and Industrial Chemistry, University of Genova, via Dodecaneso, 31, 16146, Genova, Italy
[e] Borealis Polyolefine GmbH, Innovation Headquarters, St. Peterstrasse 25, 4021, Linz, Austria

ARTICLE INFO

Keywords:
Polypropylene/(polyethylene terephthalate) blends
Compatibilization
Mechanical properties
Ethylene terpolymer
Reactive compatibilization
Interphase
AFM-IR
^{1}H NMR

ABSTRACT

The increasing global plastic production has created an urgent demand for energy-efficient processes to transform mixed plastic waste into value-added products via upcycling. Compatibilization of polypropylene (PP) and poly(ethylene terephthalate) (PET), two used semi-crystalline polymers in industry, is investigated in this study. We evaluate the effectiveness of an ethylene-butylene-acrylate terpolymer (PTW) at different contents in a 70/30 PP/PET blend, examining the resulting physico-chemical characteristics. Adding PTW as compatibilizer significantly reduces the droplet size in the PP/PET blend, improving rheological and mechanical properties. Remarkably, the blend containing 1.5 % PTW exhibits maximum enhancement in mechanical properties. To understand deeply the chemical compatibilization mechanism, Fourier transform infrared spectroscopy (FTIR-ATR), Atomic Force Microscopy combined with infrared spectroscopy (AFM-IR), and Proton Nuclear Magnetic Resonance Spectroscopy (^{1}H NMR) techniques were employed. The compatibilizer was located at the interphase, and the chemical reaction using AFM-IR and ^{1}H NMR was tracked. These advanced techniques prove the chemical compatibilization mechanism in PP/PET blends with PTW. These findings contribute to understanding the compatibilization processes, offering valuable guidance for developing efficient upcycling processes for mixed plastic waste.

1. Introduction

Plastics play a critical role in modern society, with a worldwide production expected to surpass 700 million metric tons by 2030 [1,2]. Unfortunately, roughly 42 % of these plastics are used for packaging that is ultimately discarded, posing significant environmental concerns [3]. To address this challenge, scientists are exploring innovative ways to upcycle mixed plastic into new products with improved properties [4]. One promising approach involves blending immiscible polymers, which constitute a significant portion of plastic waste. However, immiscible blends exhibit poor mechanical properties, such as a lack of adhesion at their interfaces, that hinder upcycling efforts [5]. Nevertheless, the mechanical recycling of such polymers can be improved by employing compatibilizers that reduce interfacial tension and refine the obtained morphology while improving the adhesion between components, thereby opening avenues for the cost-effective production of upcycled

* Corresponding author. POLYMAT and Department of Advanced Polymers and Materials: Physics, Chemistry and Technology, Faculty of Chemistry, University of the Basque Country UPV/EHU, Paseo Manuel de Lardizabal 3, 20018, Donostia-San Sebastián, Spain.
** Corresponding author.
*** Corresponding author.
E-mail addresses: dario.cavallo@unige.it (D. Cavallo), davide.Tranchida@borealisgroup.com (D. Tranchida), alejandrojesus.muller@ehu.es (A.J. Müller).

https://doi.org/10.1016/j.polymertesting.2023.108293
Received 16 October 2023; Received in revised form 13 November 2023; Accepted 28 November 2023
Available online 10 December 2023

high-performance materials [6].

Mechanical recycling is a practical method that makes functional materials while supporting the growth of a sustainable worldwide plastic market [7]. Although Polypropylene (PP) and Polyethylene Terephthalate (PET) are semicrystalline polymers that are relatively easy to separate from waste streams because of their intrinsic properties, in specific cases, such as in packaging structures like multilayered film materials, it is important to use mechanical reprocessing with additives as a cost-effective tool rather than sending for energy recovery [8]. In this context, when PP and PET are blended, they present incompatible characteristics because both components are highly immiscible, as PP is non-polar and PET is a polar material [9]. In the melt phase, they tend to separate, forming a clear domain segregation. Therefore, the high proportion-polymer (matrix phase) will contribute to most properties, while the smaller proportion (dispersed phase) develops micron or sub-micron domains, which contributes synergistically to improving certain specific properties [10]. However, the obtained mechanical properties are inferior, without good adhesion at the interphase between components.

In recent years, there have been several studies on the use of different compatibilizer agents for PP and PET blends [9,11–21]. These studies have examined different polyolefins grafted with various groups that interact with the polar segments of PET or react with the end groups of PET. The most effective compatibilizers reported are maleic anhydride-grafted polypropylene (PP-*g*-MAH) [18], glycidyl methacrylate-grafted polypropylene (PP-*g*-GMA) [22], which interlocks with the PP phase, and at the same time, the reactive MAH or GMA groups interact or react with the PET phase; also ethylene-propylene-diene monomer (EPDM) [11] rubber materials have been reported. For instance, Van Kets et al. [22] and Guadagnini et al. [23] investigated the stabilization of PP/PET blends. They found that adding poly(styrene-*co*-(ethylene-butylene)- styrene) grafted with maleic anhydride (SEBS-g-MAH) and SEBS-g-MAG, respectively, enhanced the mechanical performance and stabilized the properties during multiple reprocessing steps that simulated mechanical recycling. However, using SEBS may pose a critical problem related to its degradation. According to Kim et al. [24], the multiple processing conditions of blends with SEBS reduce the overall molecular weight of the system, promoting molecular mobility in the chains that have undergone degradation. This results in the segregation of styrene during the process [24]. Given this scenario, it becomes crucial to investigate alternative compatibilizers. This exploration addresses issues regarding styrene segregation during the recycling processes and concerns related to occupational health and safety (HSE).

Other polyolefin/PET blends, such as PE/PET, have also been studied. Tang et al. [5] investigated these blends' compatibilization mechanism using modifiers containing epoxy and carboxyl reactive groups. Adding an ethylene-butylene-acrylate terpolymer (PTW) to this blend resulted in a 4-times increase in elongation at break and a 6-times increase in toughness. They also provided valuable information about the location of the compatibilizer by the analysis via FTIR. Also, Kaci et al. [21] explored the mechanical and morphology characteristics of virgin and recycled PE/PET blends in different proportions. Adding a terpolymer-based compatibilizer as ethylene-butyl acrylate-glycidyl methacrylate (EBGMA) reduces the dispersed phase size from large PET aggregates (10–50 μm) in uncompatibilized samples to finer morphology obtained (1–5 μm) in the compatibilized ones, resulting in the improvement of the interfacial adhesion and the increase in the impact strength.

During the blending process, numerous variables intervene, such as temperature, shear, and extrusion geometry. Hence, it is difficult to determine how the compatibilizer diffuses and interacts with the blend components. This raises the question of the location of the compatibilizer after processing and its interaction with both phases. Another critical question is whether an optimal amount of compatibilizer enhances the properties of the blend. Usually, when there is a reduction in the blend's dispersed phase size, it is assumed that the compatibilizer migrated to the interface. Still, its exact location at the molecular level usually is not shown. Also, the mechanism by which the compatibilizer acts, for instance, by chemical reaction or just by chemical affinity, is unclear. As far as the authors know, the exact location and chemical interactions of PTW molecules within the 70/30 PP/PET blend have not been studied in detail and is presented here for the first time. This composition was chosen to guarantee that PP acts as the matrix, with PET in the dispersed phase, influencing the overall material properties. The optimization of the material properties and the compatibilizer location results from this system should also be relevant for blends with a reduced PET content. Consequently, the findings from this investigation can be extrapolated to a broader spectrum of PP/PET combinations, emphasizing their significance in either recycling PP/PET materials or promoting new, improved materials from virgin resins.

The present paper studied the impact of adding ELVALOY™ PTW, a commercial ethylene terpolymer-based compatibilizer, to a 70/30 PP/PET blend. The primary aim is to precisely determine the compatibilizer's location within the blend and clarify the compatibilization mechanism responsible for the improved morphological, mechanical, and rheological properties observed. Different PTW concentrations are evaluated through various characterization tools. The study of the optimal compatibilization content and compatibilization mechanism can be used to improve the mechanical properties and performance of similar blended systems and use the final material in different applications, such as in pipes [25] or packaging materials [26].

2. Experimental section

2.1. Materials

Borealis Polyolefine GmbH (Linz, Austria) and Novapet (Zaragoza, Spain) supplied the materials used in this study. Specifically, isotactic polypropylene with BNT nucleating agent (HD905CF) was used, with a Melt Flow Rate (MFR) of 6.5 g/10 min (230 °C/2.16 kg). Polyethylene terephthalate (PET) from Novapet (Novapet CR) was also used, with an intrinsic viscosity of 0.80 dL/g in m-cresol. Polypropylene and polyethylene terephthalate were blended in a weight ratio of 70/30. To improve compatibility between the two materials, a compatibilizer agent, Elvaloy PTW (named PTW hereafter), from DOW (Tarragona, Spain), with a melt index of 12 g/10 min, was employed in different proportions in the neat blend as 0.3, 0.6, 0.9, 1.5, 3 and 4.5 %. For example, the composition of the blend containing 0.6 % of compatibilizer will be PP/PET/PTW (70/30/0.6).

To study the blends' thermal behavior, mechanical properties, morphology, rheology, and chemical characteristics, melt compounding in a COLLIN ZK25 co-rotating twin-screw extruder-kneader (Collin, Maitenbeth, Germany) at a constant temperature of 270 °C and 200 rpm (D = 25 mm and L/D = 30) was used. The blends were then injection molded into tensile (ASTM D638, type IV, thickness 2 mm) and impact (ASTM D256, thickness 3.2 mm) specimens using a BATTENFELD BA-230E injection molding machine (Wittmann-Battenfeld, Vienna, Austria) with a screw diameter of 18 mm and L/D ratio of 17.8 mm. Before the extrusion and injection molding, PET and the blends were dried for 48–72 h at 80 °C in an air-circulation oven. Additionally, mixtures of low molecular weight compounds, namely ethyl acetate/cyclohexane at different compositions, were prepared for FTIR-ATR measurements.

2.2. Methods

2.2.1. Scanning electron microscopy (SEM)

The morphology of the blends was examined by Quanta 200F scanning electron microscope (Thermofisher, Vienna, Austria) operating at 5 kV. Before observation, injection molded tensile test samples were cut perpendicular to the machine direction (MD) using a Leica EM UC7

microtome at −60 °C (Leica, Wetzlar, Germany) and then etched in a 1 % $KMnO_4$ solution in 85 % H_2SO_4 for 15 min. Afterward, the samples were washed with distilled water and stirred in 30 % H_2O_2 solution for 10 min. A subsequent wash with distilled water was performed. Finally, the samples were rinsed with acetone. Then, the etched samples were sputter-coated with a Pt layer in a Quorum Q150TS Plus equipment. This process allows etching the dispersed PET phase, allowing the characteristic diameter to be evaluated with the resulting obtained hollow structures. The number and volume average diameters were calculated using the following equations [23].

$$d_n = \frac{\sum n_i d_i^2}{\sum n_i d_i} \quad (1)$$

$$d_v = \frac{\sum n_i d_i^4}{\sum n_i d_i^3} \quad (2)$$

Where n_i is the number of particles of diameter d_i. At least 200 particles were measured.

2.2.2. Transmission electron microscopy (TEM)

TEM analysis was conducted using a TECNAI G2 20 TWIN electron microscope (Thermofisher, Vienna, Austria), operated at 120 kV and equipped with a LaB_6 filament. Samples were prepared from injected tensile test specimens. Ultrathin films with a thickness of approximately 80 nm were obtained at a temperature of −50 °C using a cryo-ultramicrotome device (Leica EMFC6) equipped with a diamond knife. The cut was perpendicular to the machine direction (MD). These ultrathin sections were then placed onto 300 mesh copper grids.

2.2.3. Fourier-transform infrared spectroscopy-Attenuated total reflectance (FTIR-ATR)

FTIR-ATR spectra of the blends were collected in a Nicolet 50 spectrometer (Thermo Scientific, Vienna, Austria) equipped with a single reflection diamond ATR device. 128 scans were averaged at a spectral resolution of 4 cm^{-1}. To ensure that the PET was in the amorphous state, the inner part of a tensile specimen was melted at 260 °C for 2 min, and afterward, a pressure of 10 Tons was applied for 2 min. Samples were drastically cooled and placed in liquid nitrogen for 2 min. FTIR-ATR spectra were recorded after the samples were at room temperature. Three spectra were recorded for each sample, and their average was analyzed. During this analysis, we ensure PET is in the amorphous state because crystallinity can introduce variability in spectra due to differences in molecular orientation and packing. This variability can complicate the interpretation of FTIR spectra. Ensuring the amorphous state minimizes these effects, leading to a more straightforward interpretation of the FTIR data.

In addition, transmission FTIR was also recorded in the solid state using a Bruker Vertex 70 FTIR spectrometer (Massachusetts, United States). Spectra were recorded on 25 × 25 mm^2 films of 300 μm thickness prepared by compression molding at 260 °C, using a spectral range of 5000–500 cm^{-1}, an aperture of 6 mm, a spectral resolution of 2 cm^{-1}, 16 background scans, 16 spectrum scans, an interferogram zero filling factor of 64, and Blackmann-Harris 3-term apodization.

2.2.4. Atomic force microscopy combined with IR spectroscopy AFM-IR

In this study, injection-molded tensile specimens were analyzed using atomic force microscopy infrared (AFM-IR) measurements [27,28]. Sample preparation followed our previously described protocol for AFM-IR polymer analysis [29,30]. Leica EM-UC7, equipped with a Leica EM FC7 cryo-chamber (Wetzlar, Germany), was used to ultra-cryo-microtome the samples perpendicular to the machine direction (MD) at a low temperature of −100 °C. The resulting sections were then placed on ZnS substrates from Crystran with dimensions of 13 mm diameter and 1 mm thickness.

AFM-IR measurements were conducted using a Bruker nano-IR 3s instrument coupled with a MIRcat-QT external cavity quantum cascade laser array (EC-QCL) from Daylight Solutions (San Diego, United States). Spectra were acquired in the range of 910 cm^{-1} to 1950 cm^{-1} using AFM-IR in tapping mode and a heterodyne detection scheme. The cantilever was driven at its second resonance frequency (f2 ≈ 1450 kHz), while the AFM-IR signal was demodulated at the first resonance frequency (f1 ≈ 225 kHz) using a digital lock-in amplifier (MFLI, Zurich Instruments). The laser repetition rate was fL = f2 − f1 ≈ 1225 kHz. Gold-coated cantilevers (Tap300GB-G from BudgetSensors) with a nominal first free resonance frequency of 300 ± 100 kHz and a nominal spring constant between 20 and 75 N m^{-1} were employed. The laser source operated at a 15 % duty cycle for uncompatibilized samples and 20 % for compatibilized samples, delivering laser pulses with a peak pulse power of up to 500 mW. The laser power was adjusted between 8 % and 15 % of the original power using metal mesh attenuators (before beam splitter, nominal splitting ratio 1:1). Three spectra were recorded at 1 cm^{-1} spectral resolution for each location. Dry air generated by an adsorptive dry air generator was used to purge the instrument and all beam paths.

2.2.5. Proton nuclear magnetic resonance (^1H NMR) spectroscopy

^1H NMR spectroscopy was conducted at 400 MHz in solution-state. Neat PP, PET, and PTW, together with uncompatibilized and compatibilized samples (PP/PET 70/30 and PP/PET/PTW 70/30/1.5), were dissolved in trichloroethylene (TCE-d_2) at a temperature of 140 °C, with approximately 200 mg of the sample dissolved in 3 ml of TCE-d_2 in 10 mm NMR tubes. Butylated hydroxytoluene (BHT) was added to the solution to prevent sample degradation. ^1H NMR spectra were recorded for the dissolved samples at 125 °C using a standard spectroscopic pulse sequence (e.g., zg30). Due to the low signal-to-noise ratio (SNR) of suspected signals, longer acquisition times were employed, with acquisition parameters set at d1 = 53 ns and 512 scans accumulated. The acquired ^1H NMR spectra were subsequently processed manually.

2.2.6. Differential scanning calorimetry (DSC)

A PerkinElmer DSC 8000 (Waltham, Massachusetts, United States) under an ultra-high purity N_2 atmosphere was utilized to investigate the thermal properties of the samples. The equipment was first calibrated with indium and tin standards to ensure accurate results. Approximately 5 mg of the sample was placed in aluminum pans for testing. Differential scanning calorimetry (DSC) was performed, and the PerkinElmer Pyris software® was used to analyze the data obtained from the DSC measurements. Before sample measurements, all neat and blended materials were dried under vacuum at 90 °C for 3 days. Standard heating-cooling-heating DSC measurements were conducted to obtain the necessary information. Specifically, the first heating cycle was carried out from 25 to 270 °C at 10 °C/min. The samples were then kept at this temperature for 3 min to erase the thermal history, and then a cooling step down to 0 °C was performed at 10 °C/min. Finally, the samples were heated to 270 °C at 10 °C/min to complete the measurement process.

2.2.7. Mechanical properties

Tensile measurements were performed using an INSTRON 5569 universal testing machine (Norwood, MA, United States) following the ASTM D638 standard. A 10 mm/min crosshead speed was employed. The final values reported are the average of five valid measurements.

In addition, the Izod impact resistance of the materials was also evaluated using a CEAST 6548/000 pendulum under the ASTM D256 standard. Notched specimens were used in the experiments, and the notches (with a depth of 2.54 mm and a radius of 0.25 mm) were carefully machined after injection molding. Seven valid experiments were conducted to ensure accuracy, and the final values reported are an average of these experiments.

2.2.8. Rheology characteristics

Rheology behavior was investigated in the linear viscoelastic regime

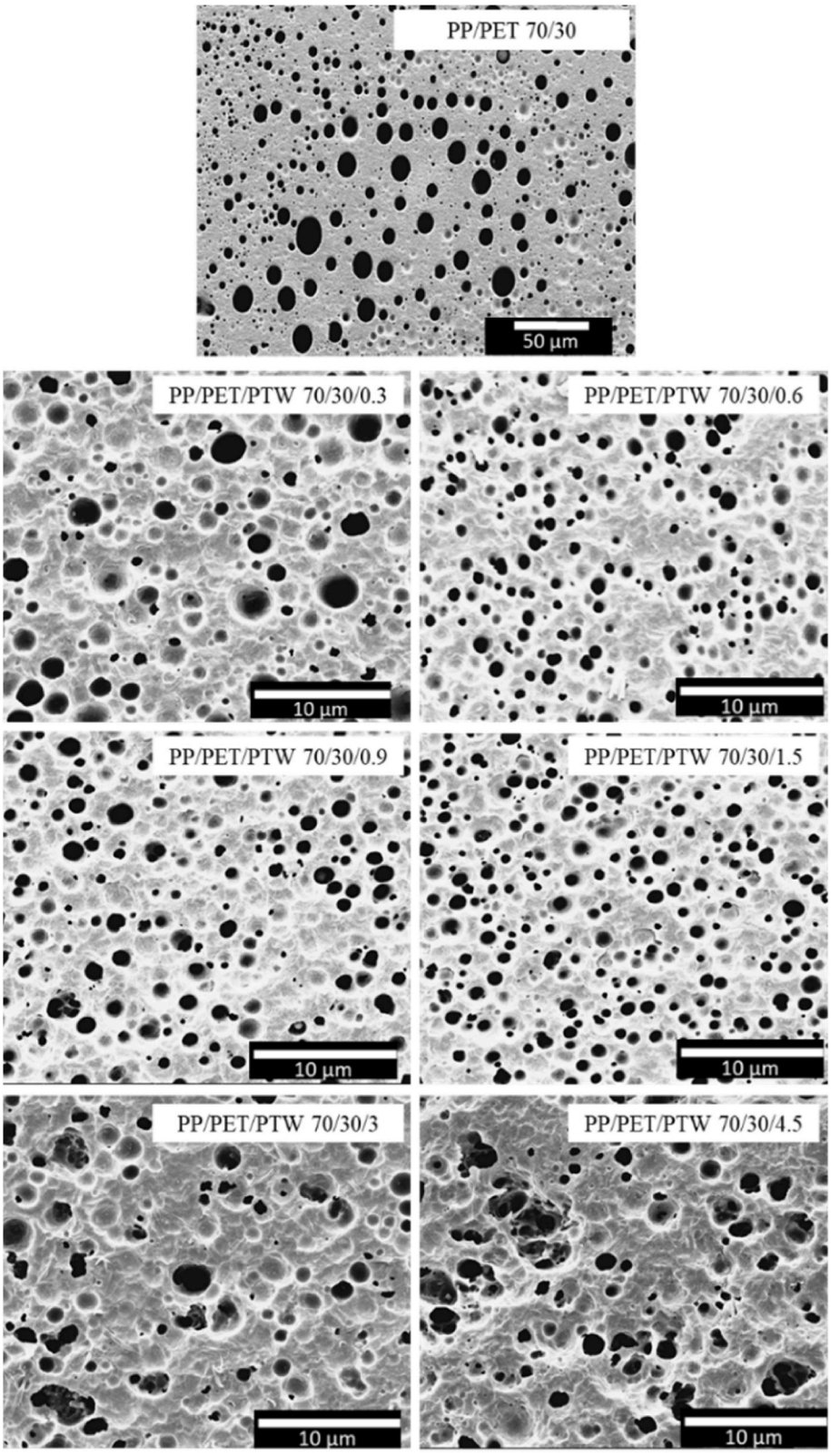

Fig. 1. SEM images of compatibilized PP/PET with PTW at different compatibilizer content after chemical etching (see experimental section).

with an ARES G2 rheometer (TA instruments, New Castle, DE, United States) under nitrogen flow in parallel plates with a diameter of 25 mm. Frequency sweeps were carried out in the linear viscoelastic regime at 270 °C with a frequency range of 628–0.01 rad s^{-1}.

3. Results and discussion

3.1. Compatibilization mechanism

High temperatures and shear conditions could promote specific

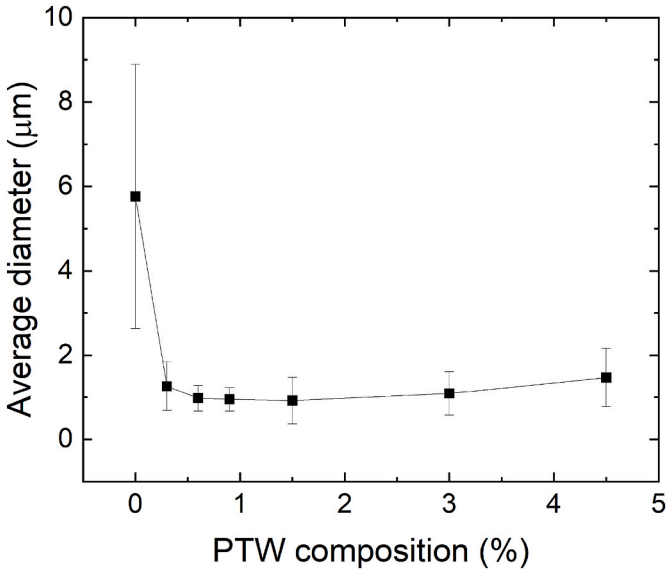

Fig. 2. The average particle size of PP/PET blends as a function of the content of PTW compatibilizer.

chemical reactions when blending PP and PET. For example, PET may undergo thermal degradation, reducing the overall properties in the uncompatibilized blend. However, high temperature and shear conditions, such as those found typically during PET processing (270–300 °C), are advantageous if a compatibilizer/modifier is added to the blend because this environment promotes diffusion and enables the possibility of chemical reactions. Enhancement in blend properties can be achieved depending on the specific chemistry of the compatibilizer used, as discussed in the introduction.

Some compatibilizers promote chemical reactions between the carboxyl group of PET and a specific functional group, referred to as a chain extender. Several functional groups can react this way, including hydroxyl, epoxy, carboxyl, anhydride, oxazoline, cyanide, and amine compounds. These groups undergo different reaction mechanisms with varying levels of reactivity and selectivity towards the hydroxyl and carboxylic end groups of PET, as well as bond stability after the reaction [31].

Incorporating chain extenders into polymer blends requires careful consideration of their compatibility with the intended reaction phase to facilitate the appropriate reaction with reactive sites. The latter is known to be susceptible to degradation for blends of polypropylene (PP) and polyethylene terephthalate (PET). Therefore, a chain extender containing polar and aromatic segments is recommended due to its greater affinity for the PET phase. Moreover, employing customized oligomeric chain extenders with high functionality and reactive phase affinity can aid in producing both linear and cross-linked chain extensions [32].

Epoxy chain extenders are similar to those found in PTW. They can react with the carboxyl and hydroxyl end groups of PET. However, the reaction rate of the carboxyl end group is dominant [33]. The carboxyl-epoxide reaction mechanism involves the opening of the epoxy ring, which interacts with the carboxyl group. The remaining epoxy oxygen is then transformed into a primary or a secondary hydroxyl, enabling further reactions with either a carboxylic acid or an epoxy. This

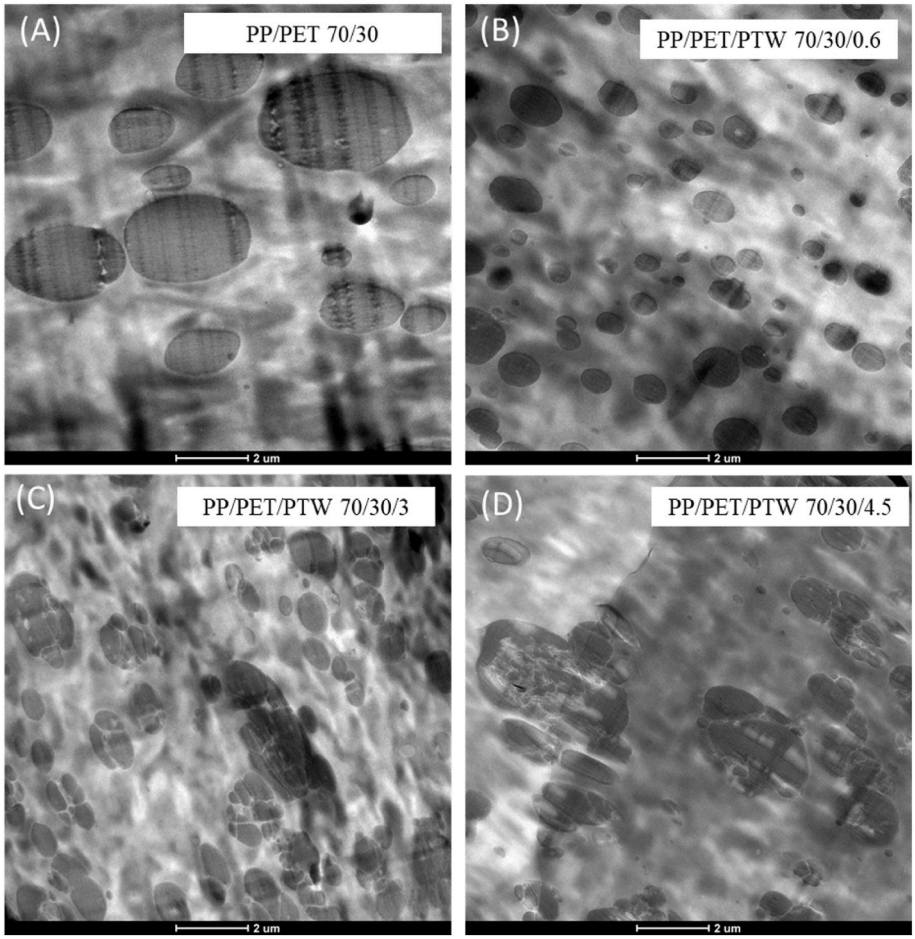

Fig. 3. TEM micrographs of (A) uncompatibilized and compatibilized PP/PET with PTW content of (B) 0.6 %, (C) 3 %, and (D) 4 %.

results in the compatibilization of both phases in a PP/PET blend [32]. To provide explanations for the chemical compatibilization and the obtained characteristics, different characterization techniques were used as follows.

3.2. Morphological characteristics (SEM and TEM)

3.2.1. SEM

The 70/30/X PP/PET/PTW blend morphology was studied by SEM. The micrographs presented in Fig. 1 clearly show a characteristic *sea-island* or matrix-droplet morphology, where the continuous PP matrix surrounds the dispersed PET phase. The hole-like structures in the micrographs represent the PET phase after the etching process. This process selectively removes the PET phase from the blends, helping to identify its precise location.

Fig. 1 shows that the addition of PTW significantly impacts the particle size distribution of blended materials compared with the uncompatibilized blend. The average particle size of the blend decreased from 5.76 μm to 0.92 μm as the amount of PTW increased, indicating its effectiveness as a compatibilizer agent. The particle size distribution values obtained from the different blends were analyzed and presented in Fig. S1 and Table S1 of the Supporting Information.

Fig. 2 shows the average dispersed particle diameter against the PTW compatibilizer content. It is possible to observe a significant particle size reduction from the uncompatibilized sample to the compatibilized blend with 0.3 % of PTW. This is because the PTW might act mainly at the interphase, reducing interfacial tension and preventing coalescence during blend preparation.

In addition, when the PTW content was increased from 1.5 % to 4.5 %, the average particle size started to increase again, although very slightly. This effect is attributed to an excess in the PTW content within the blend, which can lead to a partition of the amount of PTW between the interphase and the PET phase. This leads to losing size control since PTW may agglomerate as a third phase. When analyzing the blend with the highest PTW content (i.e., 4.5 %, see Fig. 1), a change can be noticed in the morphology pattern of the dispersed phase. Larger particles that contain smaller ones inside are visible; this confirms the overload or excess of compatibilizer, which is aggregating and losing its ability to control the dispersed phase size.

Moreover, we have conducted a one-way ANOVA analysis to demonstrate that the average particle sizes obtained from the SEM measurements at 0.3 % and 4.5 % are significantly different. The study shows a statistically significant difference between the mentioned groups ($F = 9.72$; $p = 0.0019$). For detailed information on the ANOVA results, please see Table S2 in the supplementary information.

Furthermore, it is crucial to carefully optimize the PTW content to achieve the desired dispersed phase morphology. This optimization is important because the morphology characteristics significantly affect other properties, such as the mechanical properties, as discussed further in section 3.7. In this case, the morphology analysis revealed that a compatibilizer content of 1.5 % was the most effective PTW content in controlling the particle size of the PET phase.

3.2.2. TEM

In addition to SEM analysis, TEM complemented the morphological study and checked if this technique could reveal the compatibilizer location. Fig. 3 shows the characteristic *sea-island* morphology obtained for the compatibilized and uncompatibilized PP/PET blends.

Meaningful changes in the particle size of the dispersed phase upon adding the compatibilizer PTW were observed. In agreement with SEM, the results suggest that the compatibilizer primarily acts at the interphase, improving the compatibility between the two phases because of the reduction of the PET domain size (see Fig. 3).

In addition, Fig. 3 also shows that at higher concentrations of PTW (3.0 and 4.5 %), a change in the form of the PET droplets is observed. This finding aligns with the ones from the SEM analysis, which also detected the presence of larger particles containing smaller particles within them. The presence of these larger particles with internal small particles suggests that the PTW is no longer effectively controlling the size of the dispersed phase.

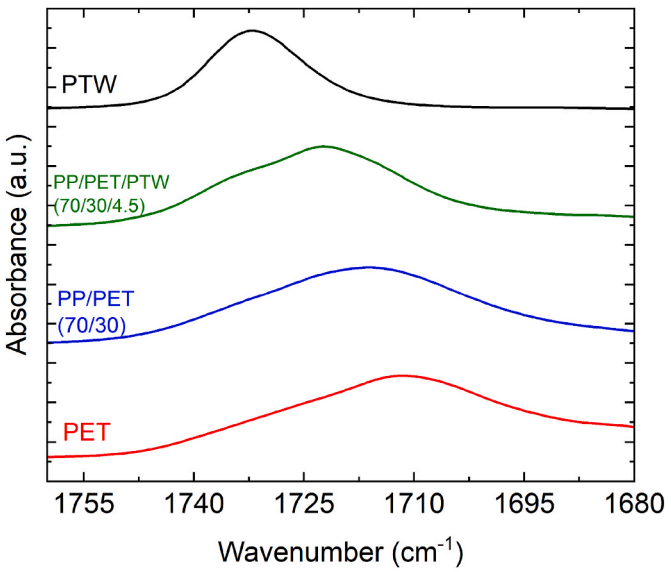

Fig. 4. Scale expanded infrared spectra of neat PET and PTW and of the PP/PET 70/30 blend without compatibilizer and with 4.5 % of PTW.

This phenomenon can be explained by the partitioning of PTW within the blend. As the PTW concentration increases beyond an optimal range, some compatibilizer starts to distribute between the interphase (the boundary between PP and PET) and the PET phase itself. This excess PTW may form aggregates, behaving as a third phase within the blend. These PTW aggregates within the dispersed phase, consequently affecting the morphology and the rest of the properties.

The morphological analysis allowed us to identify the alterations in the blend morphology caused by adding the compatibilizer. The compatibilizer appears to be present in both the dispersed phase and the interphase of the blend. Since the compatibilizer has the potential to facilitate reactive compatibilization between its reactive epoxy groups and the carboxyl groups in PET, it becomes crucial to determine the location within the blend. In order to provide further clarification regarding the location and compatibilizer mechanism (physical interaction or chemical reaction), the subsequent sections discuss the utilization of chemical analysis in conjunction with morphology assessment (such as FTIR-ATR and AFM-IR) in specific regions of the blend.

3.3. FTIR-ATR analysis

3.3.1. The reaction between compatibilizer and blend components

Elvaloy PTW is an ethylene-butylene-acrylate terpolymer that contains reactive epoxy groups. During the extrusion process, it could give rise to a covalent bond by reaction with the final hydroxyl or carboxylic acid groups of the PET. As expected, the IR bands related to polyacrylate and polyethylene are present in the infrared spectrum of neat PTW (see Fig. S2 in the supplementary information). In addition, a small absorption band, related to the epoxy ring bending at 915 cm^{-1}, appears.

Infrared spectra of the compatibilized blends show the characteristic bands related to their component materials (PP and PET) (See Fig. S3 in the supplementary information). A small shoulder related to the PTW appears in the carbonyl stretching region at 1735 cm^{-1}, see Fig. 4. Interestingly, the spectra do not show any absorption related to the epoxy bending at 915 cm^{-1}. Although other authors have considered this as evidence of the covalent link between PTW and PET [5], in our opinion, the proofs are not definitive. On the one hand, the absorbance

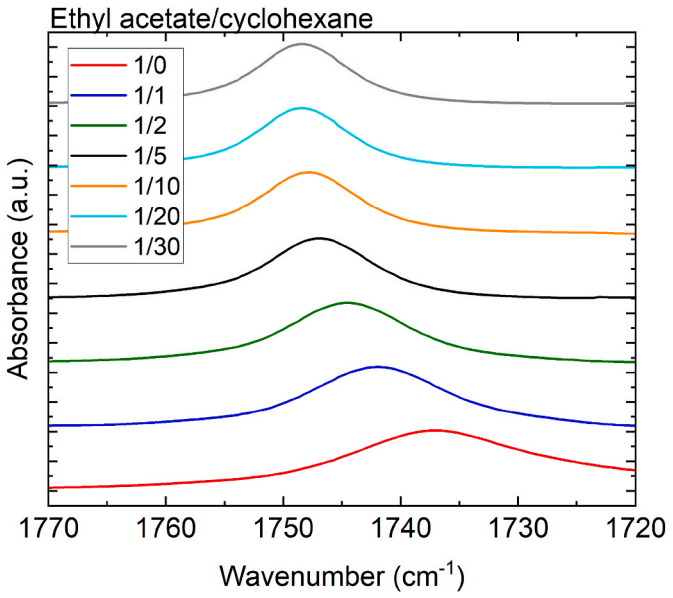

Fig. 5. Scale-expanded infrared spectra of ethyl acetate/cyclohexane different composition blends.

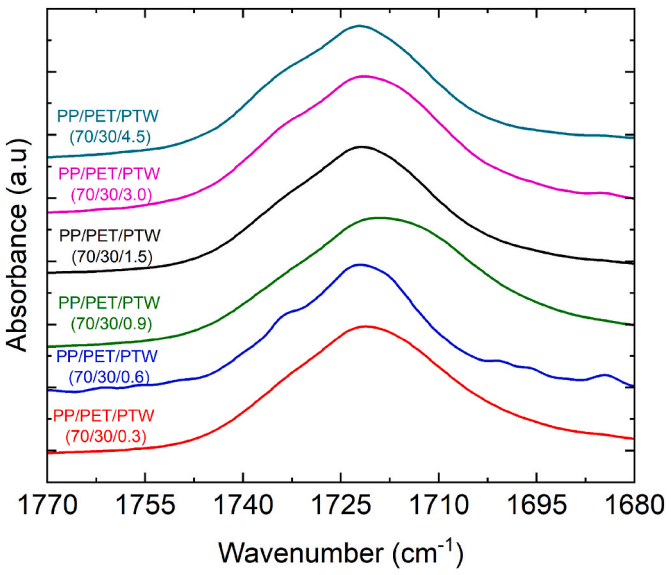

Fig. 6. Scale expanded infrared spectra of compatibilized PP/PET 70/30 blend with different amounts of PTW.

of this band in neat PTW is low; therefore, when diluted in the blend, the absorbance will be very difficult to observe. On the other hand, neat PP presents an absorption at 900 cm^{-1}, which may overlap with the epoxy bending characteristic band.

3.3.2. *Interaction between blend components*

Infrared spectra of the 70/30 PP/PET blends present characteristic bands of both components. It should be noted that the spectra were obtained after a thermal treatment to melt all PET crystals and then quickly quenched the material to avoid PET crystallization (the lack of PET crystallinity was corroborated by DSC experiments performed after fast-quenching the samples from the melt). Fig. 4 shows the scale-expanded infrared spectra in the carbonyl stretching region of neat PET and PTW and the PP/PET 70/30 blend without PTW and with 4.5 % of PTW. PET and PTW present carbonyl stretching bands at 1713 and 1733 cm^{-1}, respectively. As expected, the spectrum of the blend containing PTW presents these two bands (related to PET and PTW carbonyl stretching), while the spectrum of the uncompatibilized blend presents only the band associated with PET. Surprisingly, the band corresponding to the carbonyl stretching of the PET shifts to a higher wavenumber in the blends from 1716 to 1723 cm^{-1} in the uncompatibilized and compatibilized blends, respectively.

As infrared spectroscopy is extremely sensitive to changes in bond strength, this shift suggests that intermolecular interactions can occur between the blend components. Considering the chemical nature of the functional groups of the blend, hydrogen bonding and ionic interactions can be discarded. However, the carbonyl groups of PET can give rise to dipole-dipole interactions. When PET is mixed with PP, even if the blend is phase-separated, the carbonyl groups of the PET are diluted, and accordingly, the dipole-dipole interactions decrease. This strengthens the carbonyl bond; consequently, the carbonyl stretching shifts towards a higher wavenumber.

To confirm the effect of the dilution in a non-polar media of the carbonyl infrared band, we decided to study an analogous low molecular weight mixture of ethyl acetate/cyclohexane. Different compositions were prepared. Fig. 5 shows the scale-expanded infrared spectra in the carbonyl stretching region of these blends.

As observed, the dilution of ethyl acetate in a non-polar solvent shifts the carbonyl stretching band to higher wavenumbers. This result confirms that the shift observed in the PP/PET blend is related to the reduction of the dipole-dipole interactions.

It is worth mentioning that the shift of the carbonyl stretching vibration is higher for the blend containing a compatibilizer agent (the shift is 10 cm^{-1} compared to neat PET). This result suggests that in the compatibilized blend, the domain size is smaller, and therefore, the carbonyl is more diluted, decreasing the dipole-dipole interactions and, accordingly, a significant increase in the wavenumber of the carbonyl takes place.

Scale-expanded infrared spectra of the 70/30 blend containing different amounts of the compatibilizing agent can be found in Fig. 6.

The results show that the position of the carbonyl stretching region of the PET (excluding the sample containing 0.9 % of PTW) does not change with the content of PTW. According to the previous explanation, this means that the dilution of PET is similar in all blended samples. Although a slight increase in the particle size distribution of PET was observed when the compatibilizer composition increased, this effect is not enough to shift the carbonyl signal.

The results demonstrate that PTW reduces the domain size, but they do not provide information about where the compatibilizer is located in the blend. The second derivative spectra of the 70/30 blends with different PTW content allows the position of this absorption to be calculated and rends the following values: 1733, 1734, 1732, 1733, 1734, 1736 cm^{-1} for the samples containing 0.3, 0.6, 0.9, 1.5, 3 and 4.5 % PTW content, respectively. As mentioned, the band at 1733 cm^{-1} is due to the PTW carbonyl. This band appears at a higher wavenumber than PET due to the aliphatic nature of the PTW ester. Therefore, the band's position remains constant until the highest concentration, where a slight increase in the wavenumber is observed. As previously reported by SEM and TEM, PTW is located both at the surface of the particles and in the PET domains. Accordingly, the interaction between the PP and the PTW that increases the wavenumber of the carbonyl stretching should happen only at the droplet surface; this happens because non-polar segments of PTW interact with PP, which is also non-polar, leading to better dispersion of PET in the PP matrix. Thus, the results suggest that when increasing the PTW concentration, the part of the PTW located in the surfaces is increased.

FTIR-ATR measurements cannot confirm the covalent linkage between the PTW and the PET because of the low absorbance of the bands related to PTW. However, the results demonstrate the ability of PTW to disperse the PET domains and suggest that a fraction of the compatibilizing agent is probably at the surface of the PET domains.

To increase the absorbance of the bands related to PTW, further

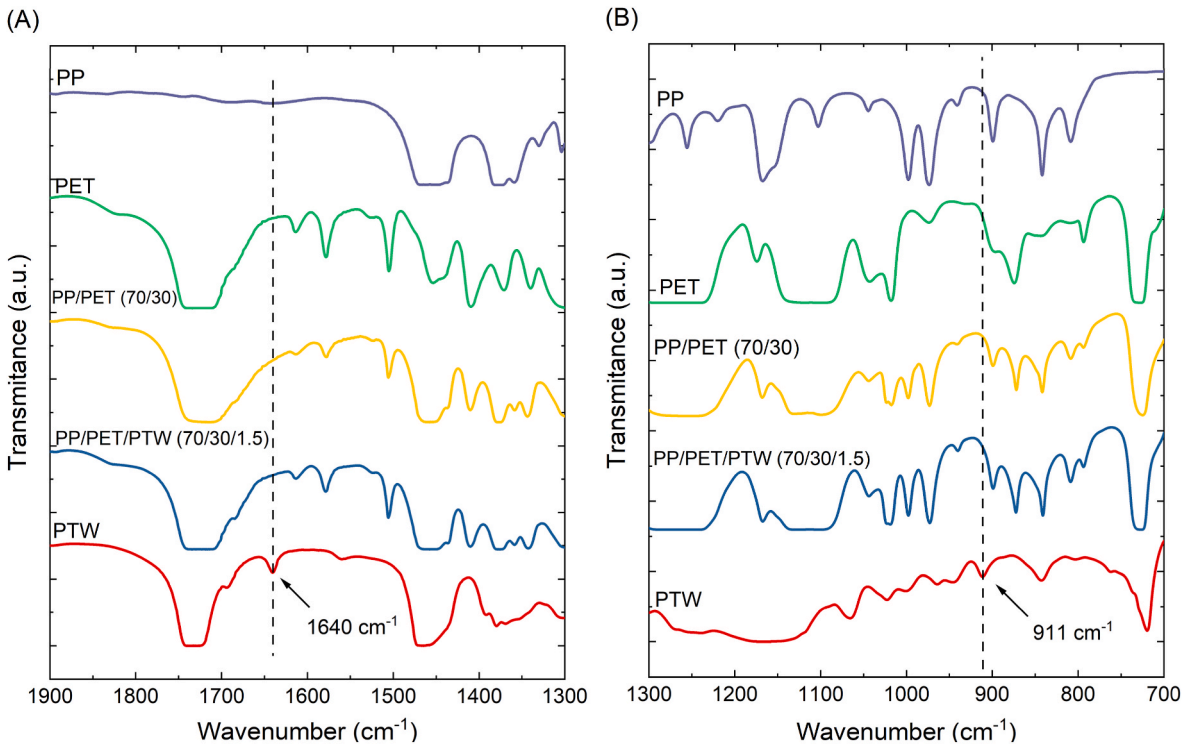

Fig. 7. FTIR spectra of neat and blended materials showing two main changes.

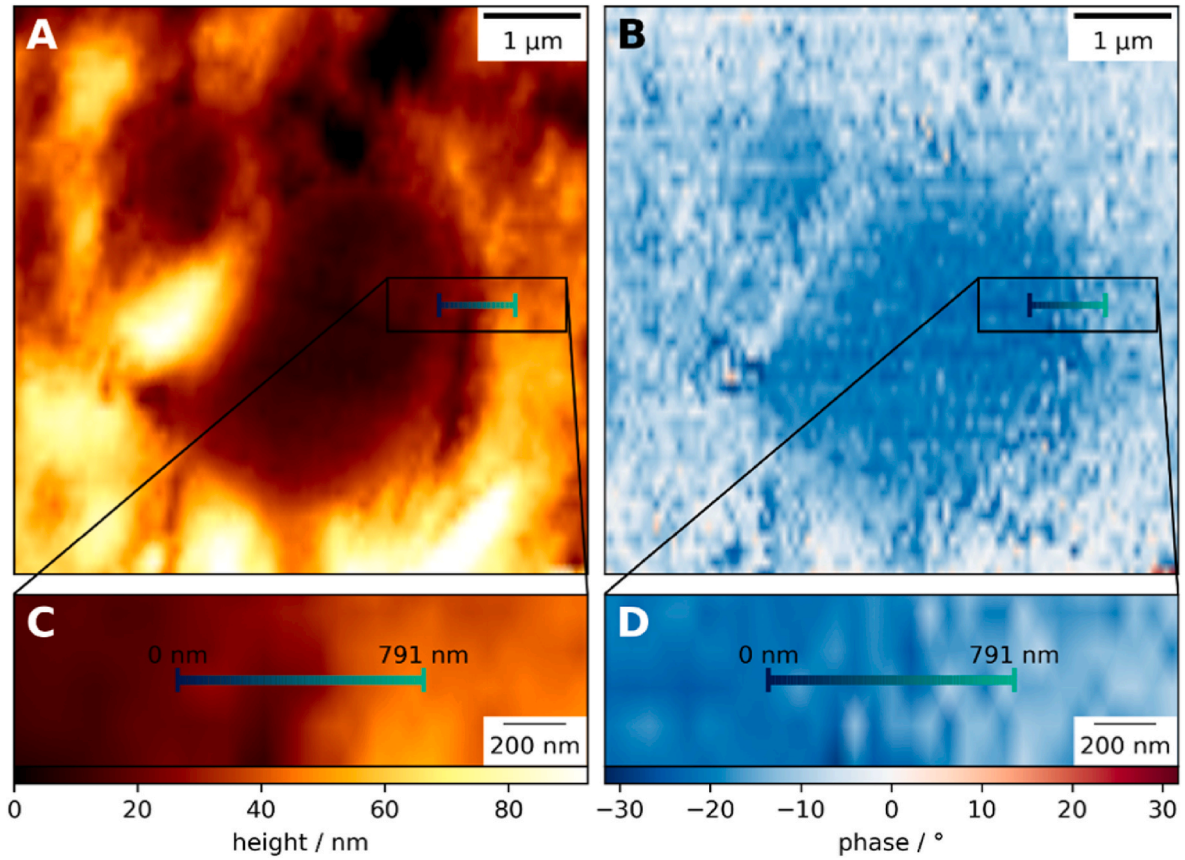

Fig. 8. AFM-IR (A) topography and (B) phase image corresponding to uncompatibilized PP/PET sample. (C) and (D) magnified areas correspond to where the spectra were taken per point across the interphase. The color of the line corresponds to the color of the spectra in Fig. S4. (For interpretation of the references to color in this figure legend, the reader is referred to the Web version of this article.)

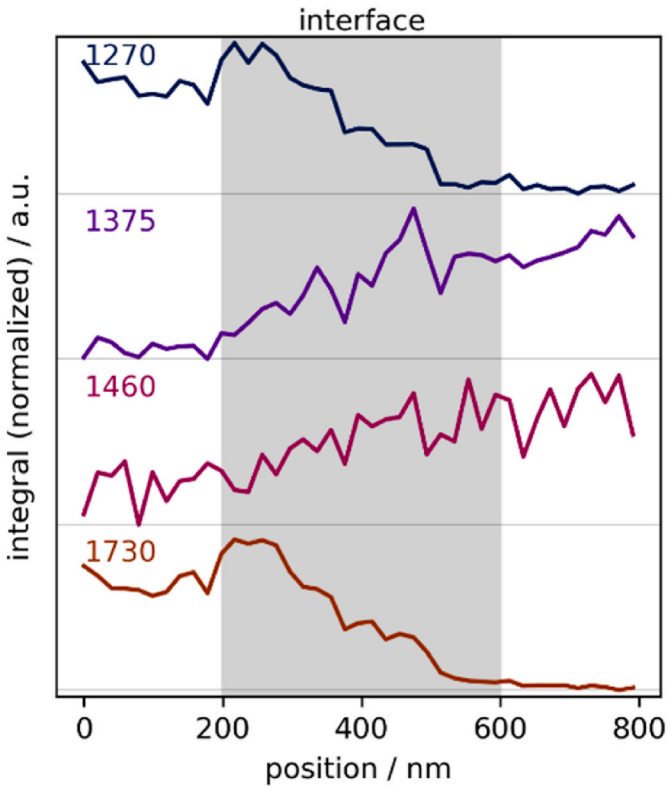

Fig. 9. Integrated marker bands showing the important change during the interphase transition. 1730 cm^{-1} corresponds to PET, and 1375 cm^{-1} corresponds to PP in the uncompatibilized blend, showing a transition within the interphase region (marked in grey).

analysis was carried out using transmission Fourier transform infrared (FTIR) spectroscopy instead of ATR measurements.

Fig. 7 depicts the resulting FTIR spectra of the neat and blended materials and the neat compatibilizer PTW. The spectra reveal two significant changes in characteristic peaks. First, in Fig. 7(A), the band at 1640 cm^{-1}, associated with vinyl unsaturated groups, is present in PTW but absent in the compatibilized (PP/PET/PTW 70/30/1.5) material. This outcome may indicate the occurrence of some reactions between the two blend components through the rupture of the vinyl double bonds; however, the low amount of compatibilizer in the blended material could make detection difficult. Secondly, in Fig. 7(B), the characteristic epoxy group at 911 cm^{-1} is absent, suggesting a chemical reaction. This result agrees with previously reported works [5,34]. However, upon analyzing the compatibilized and uncompatibilized blend, the peak at 900 cm^{-1} associated with methylene groups in PP can overlap with the epoxy signal at 911 cm^{-1} in PTW, as previously discussed in the results from FTIR-ATR measurements. As previously highlighted, this could indicate chemical compatibility at the interphase, but insufficient evidence exists. Therefore, further AFM-IR is used in the following section to elucidate the chemical reaction at the interface.

3.4. Atomic force microscopy with infrared spectroscopy (AFM-IR)

To study the specifics of the compatibilization mechanism in PP/PET blends with PTW at the nanoscale, atomic force microscopy infrared (AFM-IR) was employed. This technique provides nanoscale spatial resolution infrared spectra and images through photothermal transduction of infrared absorption [28]. The chemical information provided by infrared absorption at this high spatial resolution enables us to precisely investigate the chemical modifications occurring within the interface in the blends. By analyzing uncompatibilized and compatibilized samples, the distinct chemical characteristics were compared at the microstructural level, specifically at the interface.

3.4.1. Uncompatibilized blend PP/PET (70/30)

Topography and phase images were recorded to observe the dispersed phase distribution in the uncompatibilized blend. Fig. 8 shows clear particle segregation, where the darker color (negative phase shift) represents the PET phase, and the lighter color corresponds to the matrix PP phase. This observation follows the findings from our previous characterization using SEM and TEM.

Using the AFM image to identify the phases, a series of AFM-IR spectra was obtained across the interphase, moving from the PET phase outwards to the PP matrix phase (see Fig. 8 for location of spectra). Spectra were taken at a spacing of 20 nm, and three raw spectra were taken per position. The evaluation was conducted to see any spectral characteristic changes.

After data processing, the averaged and smoothed spectra at the individual image locations across the interface are shown in Fig. S4. Note that the 0 nm location represents the left side of the colored line in Fig. 8, and the last location at 791 nm is on the right side of the line. The spectra show a distinct trend with, most notably, the 1730 cm^{-1} decreasing and the 1375 cm^{-1} band increasing as the measurement positions move from PET towards PP.

Fig. 9 shows a distinct transition at the interfacial boundary of the PP/PET blend without a compatibilizer. This transition is characterized by a decrease in intensity of the 1730 cm^{-1} band and a corresponding increase in the 1375 cm^{-1} peak and occurs within a range of approximately 400 nm. In this case, the 1735 cm^{-1} band is associated with the PET's C═O stretching groups, and the 1375 cm^{-1} corresponds to the C–H bending in the PP phase. It is essential to notice that the intensity of the peak at 1270 cm^{-1} associated with the C–CO–C stretching in PET is also decreasing.

Marker bands for PET and PP were integrated and normalized to see the spectral changes across the measured line (see Fig. 9). The interface region marked in light grey was selected as the more significant spectral change was observed around that position. Fig. S5 also presents an enlarged form of the spectral changes in the interphase region.

Bands associated with the PET phase (1270 cm^{-1} and 1730 cm^{-1}) decrease as the tip approaches the PP phase, which demonstrates the segregation of the phases via a chemical perspective. Bands assigned to PP (1375 cm^{-1} and 1460 cm^{-1}) increase simultaneously.

3.4.2. Compatibilized blend: PP/PET/PTW (70/30/1.5)

The same approach used in the uncompatibilized blend is now used in the PP/PET/PTW compatibilized blend. First, topography and phase images were taken to obtain the particle size separation in the compatibilized blend. Fig. 10(A) shows the topography image where the phase separation is observed; however, it is also worth noting that the particle size is significantly smaller (0.6 μm) compared with the uncompatibilized blend (4.3 μm), considering just the analyzed area. This agrees with the previous morphological characterization, where it was observed that the overall particle size tuning was an effect of the compatibilizer. Fig. 10(B) shows the phase image of the compatibilized blend; it is possible to observe that the segregation of PP and PET is not distinguishable in this case. On the other hand, in the uncompatibilized blend (Fig. 8(B)), the phase image showed that it was possible to differentiate the segregation. This is because as the compatibilization took place, the particle size was smaller, and the interphase was chemically modified, being more difficult to detect in the phase image from the AFM.

Three raw spectra per each step were taken on measurement points along the colored bar marked in Fig. 10. A distance of 20 nm was used to track the chemical reaction in the compatibilized blend. The evaluation was conducted from the PET to the PP location to address any spectral characteristic change during the interphase. After data processing, the averaged and smoothed spectra at the individual image locations across

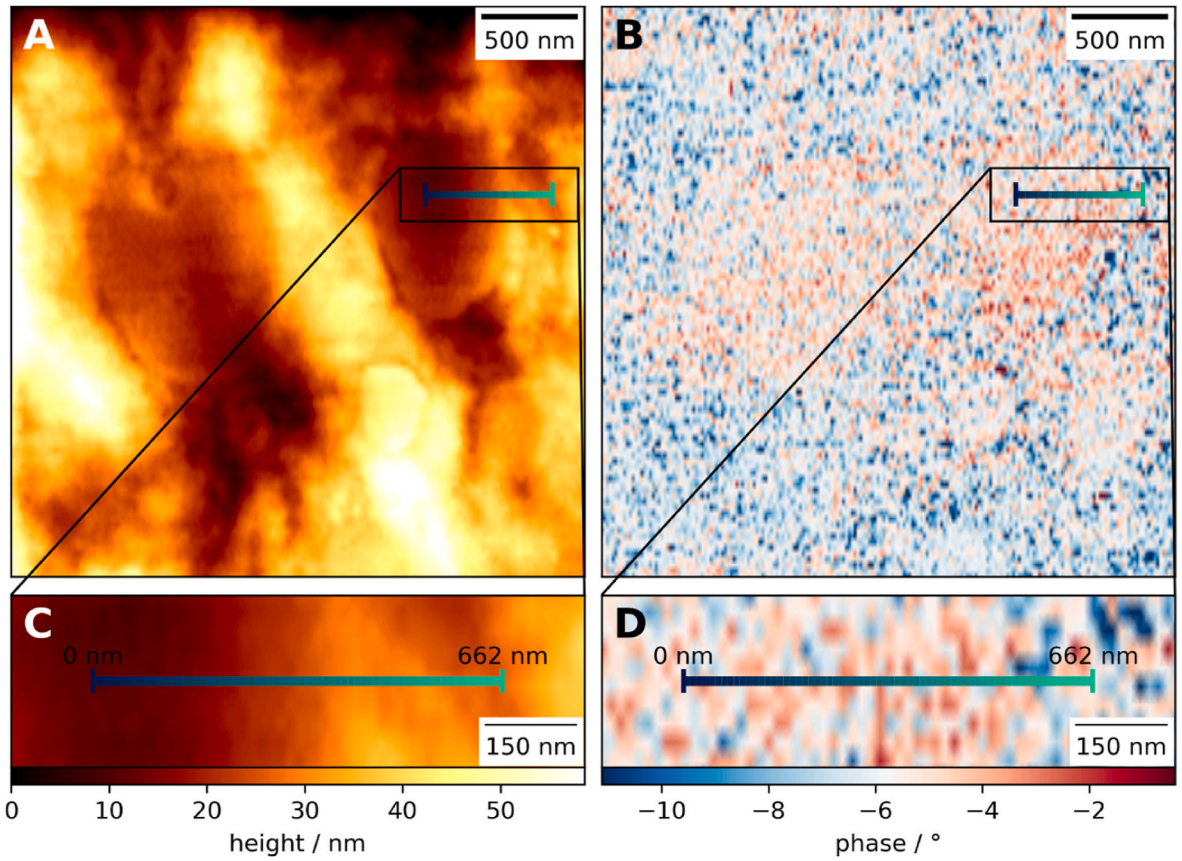

Fig. 10. AFM-IR (A) topography and (B) phase image corresponding to compatibilized PP/PET/PTW sample. The magnified areas (C) and (D) show the location spectra were taken across the interphase. The color of the line corresponds to the color of the spectra in Fig. S6. (For interpretation of the references to color in this figure legend, the reader is referred to the Web version of this article.)

the interphase are shown in Fig. S6. Note that the 0 nm location represents the left side of the bar marked in Fig. 10, and the last location at 662 nm is the right end of the bar.

In line with previous measurements, a clear transition in the characteristic bands of PP and PET within the blend was observed. As the tip approaches the PP region, a noticeable decrease in intensity is observed in the band at 1730 cm^{-1}, which is associated with carbonyl groups in PET. Similarly, a transition is seen in the band's intensity at 1270 cm^{-1}, linked to the terephthalate group in PET. Fig. 11 shows this behavior over the normalized intensity from each peak. Conversely, an increase in the band's intensity at 1375 cm^{-1}, associated with PP, was found. This further confirms the segregation of PP and PET, but in this case, within a smaller particle domain.

It is important to note that following the bands associated with the compatibilizer PTW across the interphase is challenging due to two key factors. Firstly, some bands related to PP and PET may overlap with the characteristic bands of PTW, making it difficult to distinguish them. Secondly, the spatial resolution in tapping mode AFM-IR is typically given as lower than 20 nm, meaning that all spectra might be taken too far from the compatibilizer if it forms a thin layer between PP and PET. To overcome the first issue, the 1640 cm^{-1} band was identified as the only marker for PTW that does not fully overlap with PP or PET bands. For the second issue, AFM-IR was chosen, in addition to spectroscopy: here, the laser wavelength is kept fixed at a selected band while the tip scans across the sample. This generates an image of absorption at the selected wavelength. In imaging, pixel spacing can be much smaller than in spectroscopy, enabling better detection of thin layers.

Fig. 12 shows a topography image of the PP/PET/PTW sample and three AFM-IR images collected at 1726 cm^{-1} (PET), 1375 cm^{-1} (PP) and 1640 cm^{-1} (PTW). As expected, within the droplet, a high signal for the band at 1726 cm^{-1} was observed, while outside the droplet at 1375 cm^{-1}, the absorption is strong (high AFM-IR signal). For the PTW marker band at 1640 cm^{-1}, a heterogeneous signal around the noise floor is observed. Considering a line profile across a droplet, as seen in Figs. S7 and S8, these same trends are more clearly appreciated. Furthermore, the log ratio between 1726 cm-1 and 1375 cm-1 shows that the interphase with intermediary concentrations in PET and PP appears as a halo around the droplet (see Fig. S7).

The absence of the 1640 cm^{-1} can be interpreted in two ways: first, PTW could be broadly distributed throughout the sample and thus diluted to the point where it is no longer detectable. Second, the 1640 cm^{-1} band seen in pure PTW could have been lost through chemical reaction.

3.5. Proton nuclear magnetic resonance (^1H NMR) spectroscopy

The recorded ^1H NMR spectra from neat and blended materials are presented in Fig. 13. From the obtained spectra, it was possible to assign the signals to different hydrogen atoms in the structure of each material. In the spectrum of the compatibilizer (PTW), for instance, the signals at 2.3 ppm and 4.1 ppm are associated with hydrogen atoms in the aliphatic chain of the butyl acrylate (BA) group (-C**H**-COO-, and -**CH_2**-OCO-), while the signals present in the range of 2.5–3.4 ppm correspond to the epoxy protons of the glycidyl methacrylate (GMA) group. The aromatic and aliphatic protons of PET are assigned to the signals at 8.1 ppm and 4.7 ppm, respectively.

From the uncompatibilized blend PP/PET (70/30), it is possible to observe the signals corresponding to the aliphatic protons of PP at the upfield region, along with the signals of PET, without any shift. However, when analyzing the compatibilized blend PP/PET/PTW, the

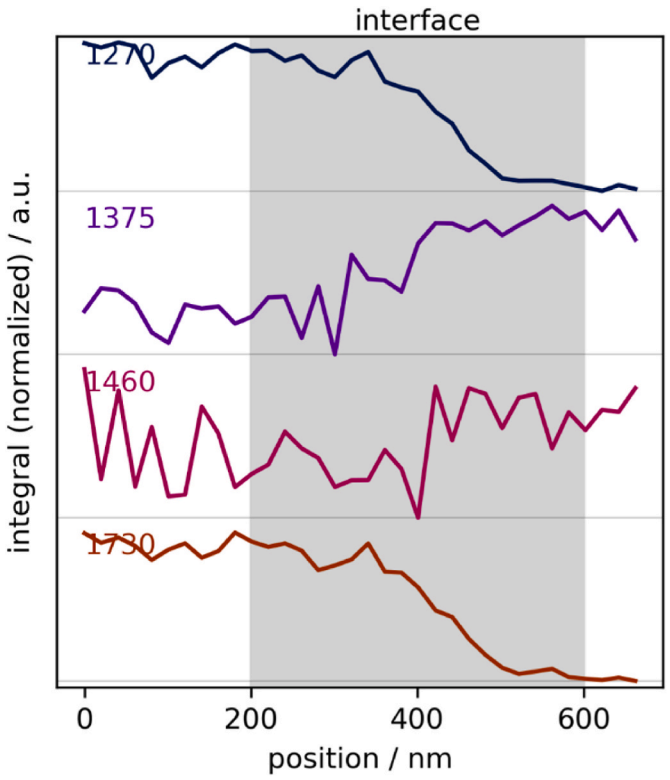

Fig. 11. Normalized marker bands at 1730 cm^{-1} from PET and 1375 cm^{-1} from PP in the compatibilized blend showing a transition within the interphase region.

signals from the BA groups associated with the compatibilizer and the lower intensity from the signals corresponding to the GMA groups can be observed. This may confirm the chemical reaction between the reactive groups in PTW and PET. However, since the amount of compatibilizer is considerably low, the dilution of it in the sample could lead to similar results.

To investigate whether the low intensity from the GMA group signals in the spectra of the compatibilized blend (PP/PET/PTW) can be attributed to dilution or effective chemical compatibilization, a complementary PP/PTW (99/1) blend was studied. Additionally, longer acquisition times were employed for the measurement to enhance sensitivity. Since PTW does not chemically interact with PP, the protonic signals of GMA and BA groups should still be observable in the ^{1}H NMR spectra. Fig. 14 compares the spectra of the compatibilized blend (PP/PET/PTW), the PP/PTW blend, and the neat compatibilizer (PTW). Notably, in the PP/PTW blend spectrum, despite the low amount of compatibilizer incorporated (1 %), the intensities of the signals in the GMA group are higher than those observed in the compatibilized blend (PP/PET/PTW) spectrum. This observation provides clear evidence that the compatibilization effect was achieved through chemical reaction between the carbonyl groups in PET and the reactive groups in PTW. Quantitative results were not possible due to the low concentration of the signals and low signal-to-noise ratio (SNR). Using ^{1}H NMR, it was possible to confirm that a decrease in intensities of glycidyl methacrylate maleic groups is present, thus supporting the hypothesis of the chemical reaction and confirming the obtained AFM-IR results.

3.6. Non-isothermal crystallization

Fig. 15 displays the results of the non-isothermal differential scanning calorimetry (DSC) cooling and heating scans measured at 10 °C/min. The scans show clear evidence of the separate crystallization and melting transitions of the phases of PET (higher temperature peak) and PP (lower temperature peak). Table 1 provides the values of the crystallization (T_c) and melting (T_m) temperatures together with the crystallization (ΔH_c) and melting (ΔH_m) enthalpies that were obtained from the analysis.

Different aspects can be highlighted regarding the crystallization and melting temperatures from the reported data. Initially, the crystallization temperature of the PP phase decreases in all the blended materials compared to neat PP at about ~3 °C. This reduction can be attributed to the transfer of impurities from PP to PET, a phenomenon reported in the literature for similar blend systems [35]. For the compatibilized blends, the crystallization temperature of PP remains relatively constant. This suggests that the addition of the compatibilizer helps to stabilize the crystallization behavior of PP, potentially mitigating the negative influence of impurity transfer.

In the case of the PET phase in the PP/PET blend, a notable increase in the crystallization temperature is observed compared to the neat PET material. This behavior can be attributed to the previous explanation about the influence of the PP component in the blend. The impurities being transferred from the PP phase act as a nucleating agent, providing additional sites for PET crystallization and accelerating the crystallization rate, thus increasing the crystallization temperature.

The addition of PTW as a compatibilizer in the PP/PET blend results in a significant decrease in the enthalpy and crystallization temperature of the PET phase compared to the neat blend. This indicates slower crystallization kinetics, as PTW is interacting chemically; it restricts the mobility and rearrangement of PET chains during crystallization.

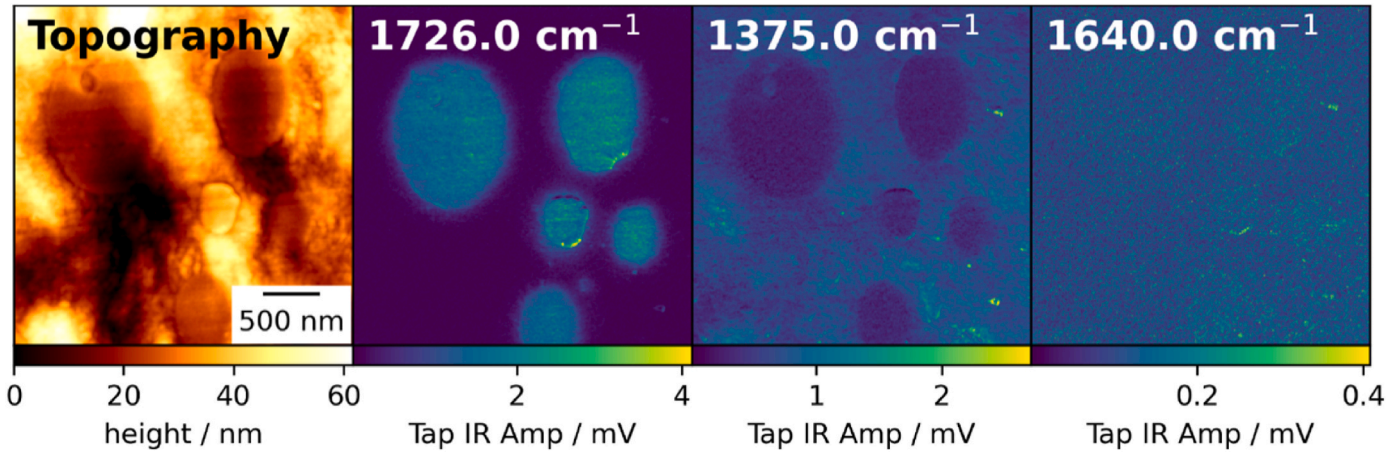

Fig. 12. Topography and IR amplitude images of marker bands from the compatibilized PP/PET/PTW blend, differentiating the contrast of domains and the interphase.

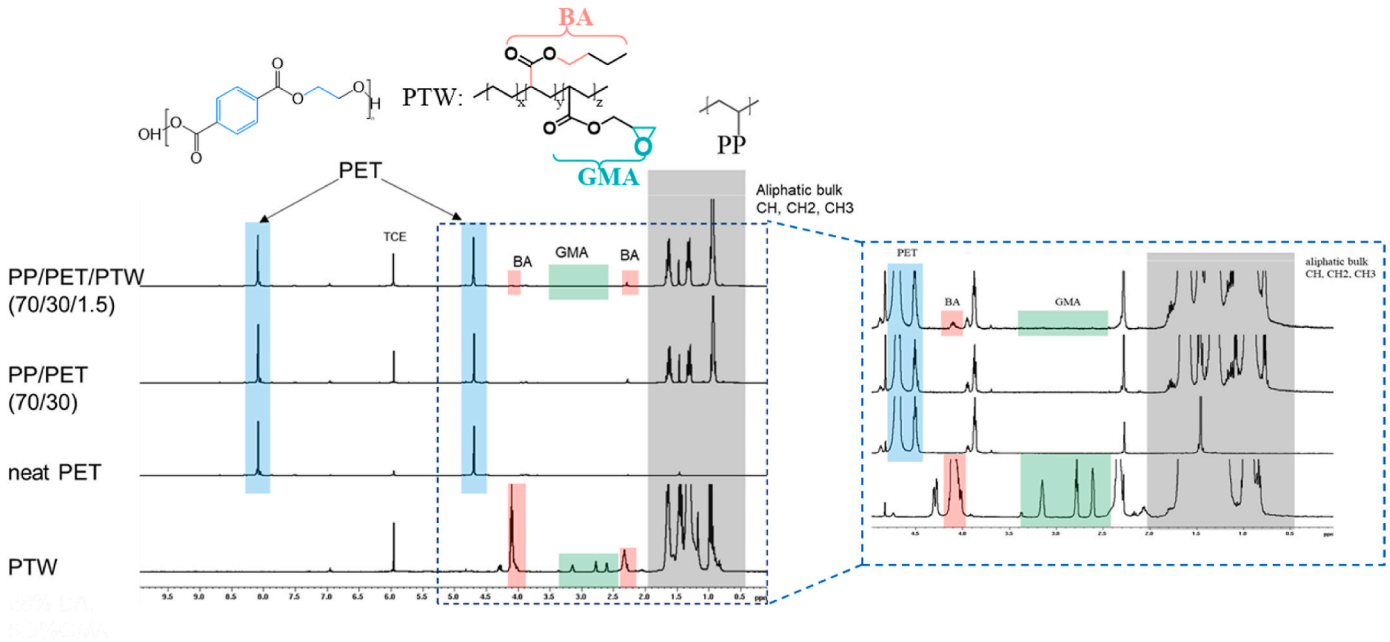

Fig. 13. NMR spectra taken from neat and blended materials with the assignment of the different H atoms to the functional groups in the materials.

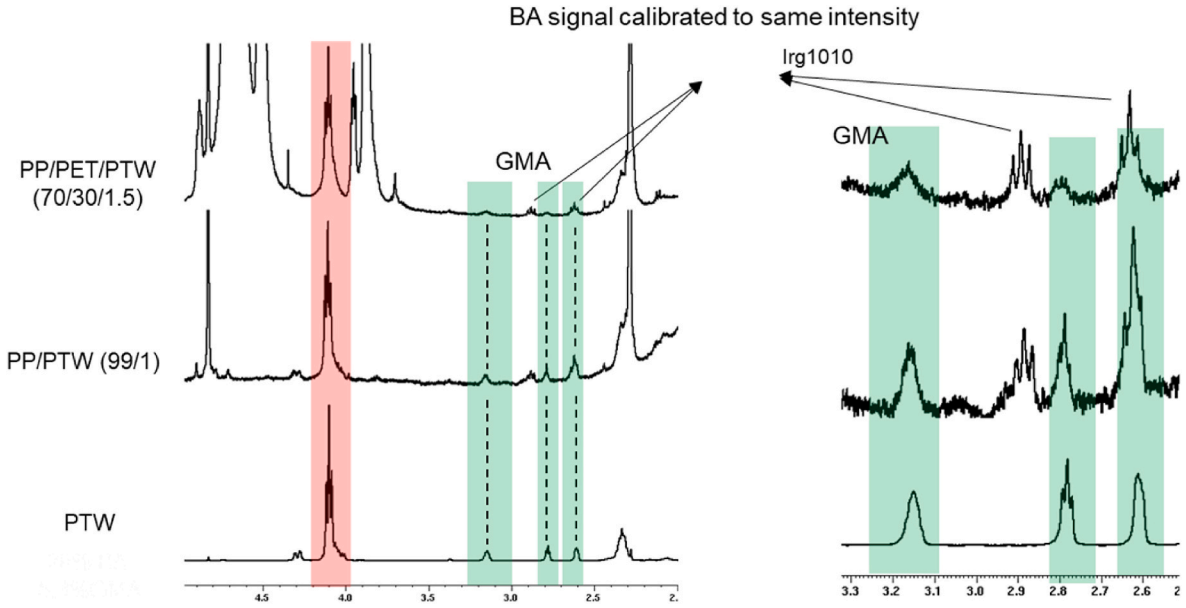

Fig. 14. Comparison of the ^{1}H NMR spectra of compatibilized blend with the PP/PTW blend and neat compatibilizer.

However, there is a trend of increasing crystallization temperature as the PTW content increases from 0.3 to 0.9 % in the compatibilized blend, which suggests PTW in intermediate concentrations potentially acts as a nucleating agent to the crystallization kinetics of PET. At a PTW composition of 1.5 %, a decrease in the crystallization temperature is observed with respect to the composition of 0.9 %, which can be attributed to the optimal value of compatibilization loading and the ability of the chemical reactions to occur.

In addition, it is noteworthy that no crystallization peak can be detected in the blends with the highest composition of compatibilizer (3.0 % and 4.5 %). This absence of a peak can be attributed to the already proven occurrence of chemical reactions between PTW and PET. The overload of compatibilizer at these compositions surpasses the optimal amount required for efficient compatibility. As a result, the ability of PET to undergo crystallization is compromised, and the characteristic crystallization peak is not observed.

Regarding the melting behavior of the studied materials, one can observe that in the PP phase, the PP/PET 70/30 decreases its melting temperature with respect to the neat polymer at about ~3 °C. Regarding the compatibilized blends, there are small changes in the melting temperatures, which can be approximated to a constant trend for both the PP and PET phases.

3.7. *Mechanical properties of the compatibilized blends*

A series of stress-strain tests in the obtained injected specimens were carried out to evaluate the tensile mechanical behavior of neat PP and PET and their blended compositions using PTW as compatibilizer. The obtained Young's modulus, yield strength, elongation at break, and impact resistance values are represented in Fig. 16.

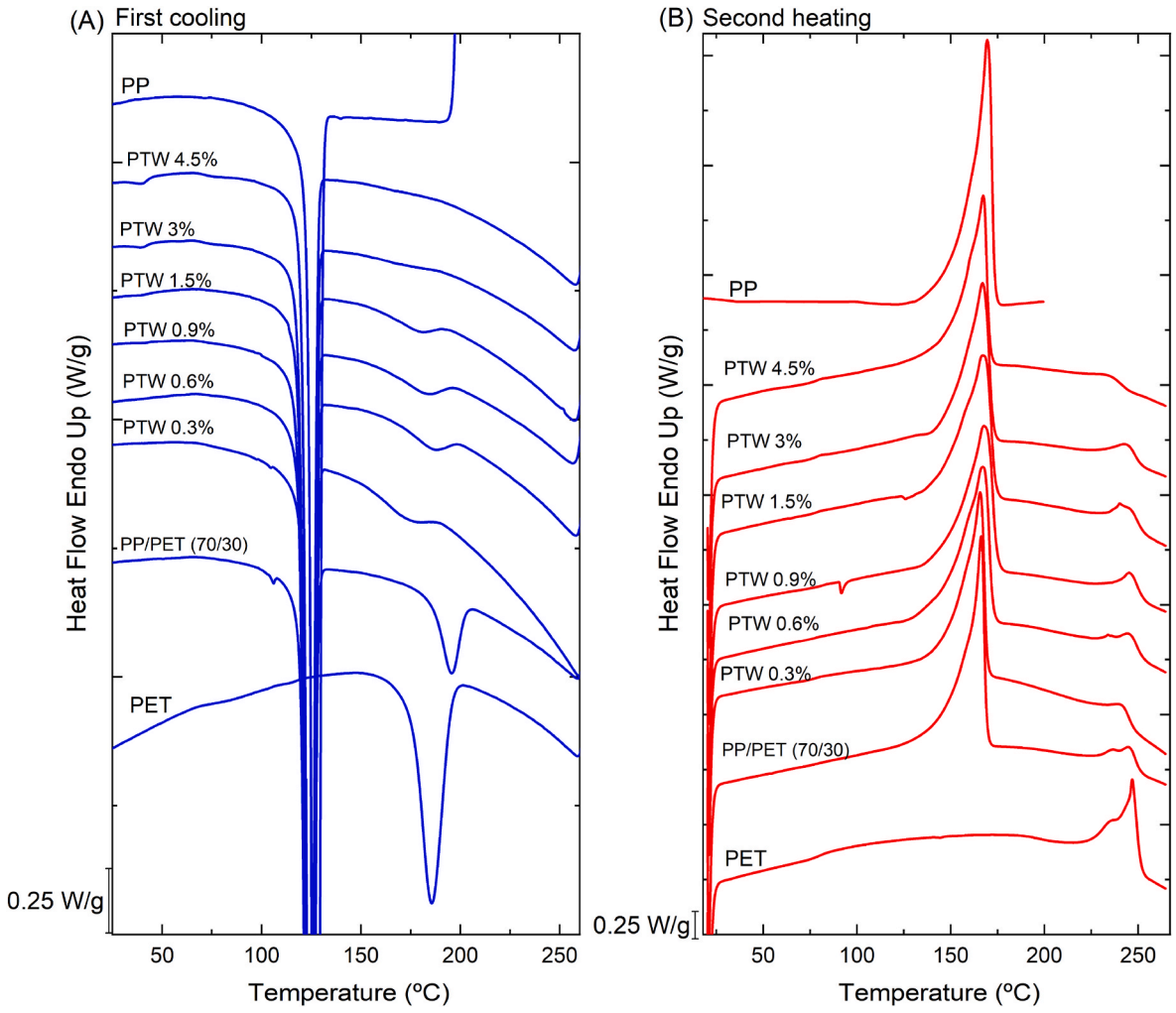

Fig. 15. (A) First DSC cooling and (B) Second heating scans for neat and blended materials.

Table 1
Obtained values for the thermal properties of the studied materials from DSC scans.

Sample	*Tc (°C)*	*ΔHc (J/g)*	*Tm (°C)*	*ΔHm (J/g)*
PP	127.5	98.65	169.6	100.76
PET	185.61	34.41	247	34.02
PP/PET 70/30	124.18a; 195.70b	68.97a; 8.91b	166.4a; 245.1b	70.80a; 7.64b
PP/PET/PTW 70/30/0.3	124.9a; 176.55b	68.50a; 3.20b	165.7a; 242.3b	68.90a; 7.49b
PP/PET/PTW 70/30/0.6	124.4a; 187.69b	72.97a; 3.35b	167.9a; 245.1b	68.89a; 7.49b
PP/PET/PTW 70/30/0.9	124.1a; 186.42b	74.49a; 3.99b	168.0a; 245.9b	68.87a; 7.24b
PP/PET/PTW 70/30/1.5	124.4a; 180.97b	74.31a; 2.65b	167.6a; 243.9b	70.38a; 7.48b
PP/PET/PTW 70/30/3.0	124.4a; -b	68.83a; -b	167.3a; 243.2b	63.75a; 7.70b
PP/PET/PTW 70/30/4.5	124.7a; -b	64.92a; -b	167.48a; -b	57.99a; 7.49b

aPP; bPET.

On the one hand, regarding the uncompatibilized PP/PET blend, the results showed that the blending of 70 % PP with 30 % PET led to a decrease in Young's modulus and stress at the yield of the blend, compared to the neat materials, since the incompatibility decreases the mechanical results significantly. Furthermore, the elongation at break of the 70/30 PP/PET blend was significantly lower than that of the neat PP or PET, showing a brittle behavior. These observations are consistent with the morphological characteristics of the uncompatibilized blend, where a poor interfacial interaction between phases and major phase separation was observed. As it is widely known [36,37], poor interfacial interactions between phases prevent the effective stress transfer from the matrix to the dispersed polymer phase, reducing mechanical properties compared to neat polymers. Moreover, as PP is a pseudo-ductile polymer, the presence of dispersed particles within the matrix may act as stress-concentrating points, especially if the interfacial adhesion is not suitable between the phases, causing an early fracture of the PP matrix and significantly reducing its initially high ductility [11,15,32]. Not in vain, the detriment of mechanical properties is a widely studied issue in various blends and is a common challenge in recycling streams, where the sorting of materials is not always efficient [38].

On the other hand, as for the effect of adding the PTW compatibilizer to the PP/PET blend, it can be observed that the addition of PTW to the PP/PET blend improved its mechanical properties. Regarding Young's moduli, Fig. 16(A) shows that the addition of PTW increases the stiffness of the PP/PET 70/30 blend. This is because, at low PTW concentrations, the blend's Young's modulus was slightly higher than that of the PP/PET blend and remained relatively constant up until a PTW content of 1.5 %. With higher compatibilizer contents (3 % and 4.5 %), the Young's modulus decreased. These results agree with the morphological observations, where a loss of the dispersed particle size control was observed above 1.5 % compatibilizer contents. The yield strength (Fig. 16(B))

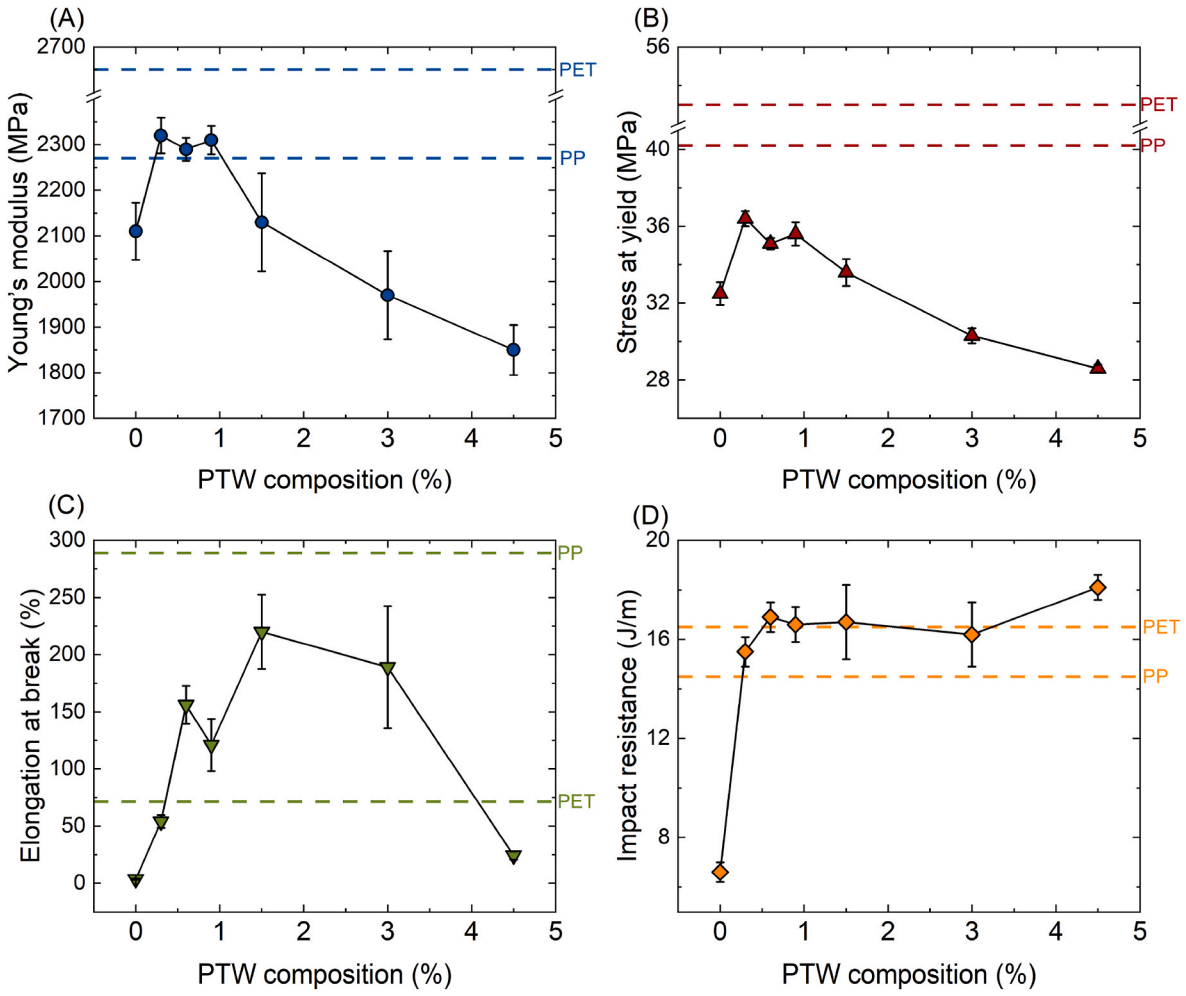

Fig. 16. Mechanical properties of blended materials as a function of PTW content where (A) represents Young's modulus, (B) the stress at yield, (C) the elongation at break, and (D) the Izod impact resistance. Discontinuous lines correspond to the value of the neat materials.

showed a very similar trend to that observed for Young's modulus, as usually happens in this type of blend [22].

As for the elongation at break, adding the compatibilizer improved the ductility of the PP/PET 70/30 blend significantly, as shown in Fig. 16(C). The blend was already ductile at a 0.3 % PTW content, and the ductility kept increasing upon PTW addition, reaching its maximum value at a PTW concentration of 1.5 %. A further increase in the compatibilizer content led to a decrease in the elongation at break. Once again, these findings agree with SEM observations, where the particle size was reported to be minimal at a compatibilizer content of 1.5 %. It is widely known that fine morphologies in immiscible polymer blends (i.e., small particle sizes and good dispersion level of the dispersed phase) lead to optimal ductility values [39,40].

In summary, at a 1.5 % PTW content, the elongation at break was maximum, while Young's modulus and yield strength remained relatively constant. These results are particularly noteworthy because adding such modifiers often improves the ductility of blends while decreasing Young's modulus or vice versa [41]. In this case, the ductility enhancement was accompanied by a moderate increase in Young's modulus and yield strength, making the blend suitable for a wide range of applications. However, further increasing the PTW concentration to 3 % and 4.5 % was detrimental to the elongation at break but beneficial to the impact resistance, with values even higher than neat PET. This high compatibilizer content promotes its aggregation, forming a third phase, as mentioned in the morphology analysis. This third phase acts as a toughening agent, contributing to the increase of the impact resistance. This suggests that the optimal concentration of PTW at which the PP/PET blend exhibits the best mechanical properties is 1.5 % of PTW. Additionally, these results agree with the previously discussed morphological changes, where the compatibilizer starts to aggregate inside the PET phase at high concentrations, resulting in a loss of control over the domain size.

With respect to the impact strength, Fig. 16(D) shows the notched Izod impact resistance values of the neat polymers and their blends. As can be observed, the addition of PET to PP results in a blend with a significantly lower impact strength than either the PP or the PET, showing a clear negative deviation from a simple rule of mixtures. Again, this is a consequence of the ineffective stress transfer from the PP matrix to the PET dispersed phase due to the coarse morphology and bad interaction between the phases, as previously discussed.

Adding PTW to the PP/PET blend increases the impact resistance behavior of the uncompatibilized PP/PET 70/30 blend. The impact resistance value increases significantly with the lowest PTW content of 0.3 %, and as the concentration of PTW increases, the impact resistance values also increase, reaching the highest value at a PTW concentration of 4.5 %. At this point, it must be noted that the PTW can act as a compatibilizer and an impact modifier [42]. Therefore, the impact strength increases with increasing the PTW content. Nevertheless, the variations observed among the compatibilized blends, and also in comparison to the neat PP and PET, are minor and fall below the experimental error; therefore, it can be considered that the impact resistance values of the compatibilized blends remain quite similar to

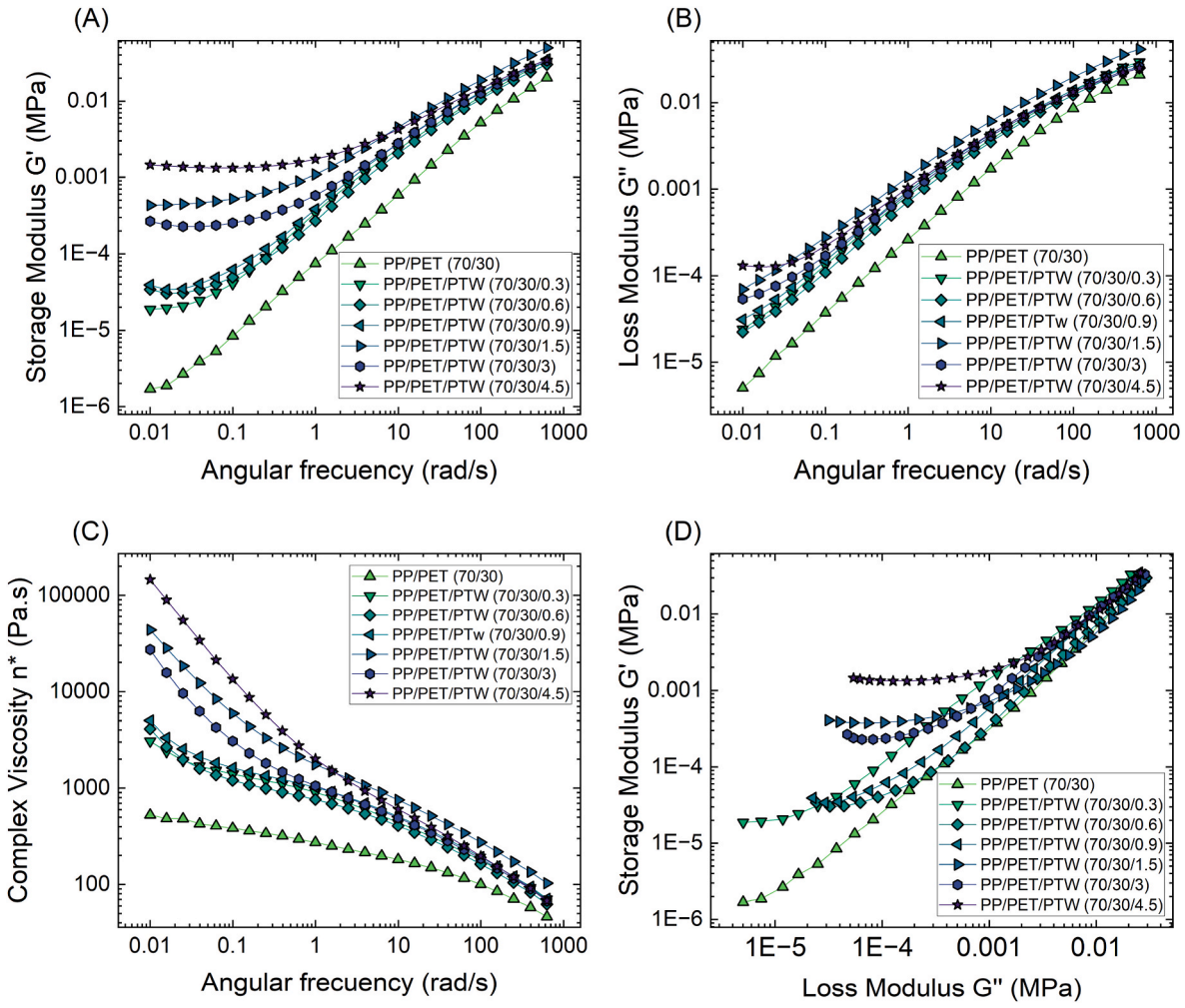

Fig. 17. Rheological properties of PP/PET 70/30 with different content of compatibilizer.

those of the neat polymers, which is a very favorable behavior.

3.8. Rheological characteristics

Small amplitude oscillatory shear measurements were conducted to investigate the rheological properties in the linear viscoelastic regime. Fig. 17 illustrates the storage modulus, loss modulus, and complex viscosity as a function of frequency and the storage modulus versus the loss modulus of the blended materials. The PP/PET 70/30 blend exhibits a viscoelastic behavior, which can be attributed to the large PET domains phase-separated within the PP matrix phase. The introduction of PTW at a low concentration increases the storage modulus, loss modulus, and complex viscosity in all frequency ranges, with a more significant effect observed at lower frequencies. These findings can be attributed to how PTW lowers the interfacial tension and prevents droplets from coalescing, decreasing droplet size and a narrower distribution of droplet sizes, as seen in the morphological analysis. Furthermore, the terpolymer's strong chemical interactions with the interphase components induce an additional contribution to the blend storage modulus.

As the composition of the compatibilizer increases, a plateau is observed in the low-frequency regime of the storage and loss modulus, and the complex viscosity increases. This plateau indicates that the blended material has achieved a more homogeneous structure due to the increased compatibility of the PP and PET phases. Higher compatibilizer content can reduce the interfacial tension and prevent coalescence, reducing droplet size and creating a more homogeneous structure, as discussed in the morphology section (see sections 3.2.1 and 3.2.2). As the morphology is tuned, the structure becomes more homogeneous, and the elastic modulus reaches a specific value and becomes relatively constant over a range of frequencies in the low-frequency regime. This results in a plateau effect observed in the storage and loss modulus in all the compatibilized blends but with a significant effect in higher compatibilizer content. This effect has been observed in the literature for similar compatibilized systems [12,43,44]. It is worth mentioning that the composition of 1.5 % of PTW is off the trend and higher than 3 %. This could be related to the optimal concentration of the compatibilizer in this blend; higher concentrations, in this case, lead to a loss of the ability to control the particle size; therefore, the structure is less homogeneous, and the storage and loss modulus decrease.

Studies conducted by Favis and colleagues, as well as other related systems [22,45], have reported comparable results on the contribution of interfacial tension and coalescence in the resulting particle size. Their research analyzed the decrease in dispersed phase size after adding SEBS-g-MA copolymer to PP/PET blends at interfacial saturation.

The ability of PTW to control and tune the general properties of PP/PET is of great importance due to numerous emergent efforts in recycling systems. Understanding complex compatibilizing mechanisms enhances neat and recycled materials by reducing associated costs and addressing the recycling challenge.

4. Conclusions

This study thoroughly investigated the addition of commercial ethylene-butyl acrylate glycidyl methacrylate terpolymer (PTW) to PP/

PET blends. Optimization determined that incorporating 1.5 % PTW into the uncompatibilized PP/PET 70/30 blend significantly improved the mechanical properties. This optimal composition consistently enhanced the overall performance of the blend.

Complementary morphological analyses using SEM, TEM, and AFM confirmed the remarkable ability of PTW to reduce domain size within the blend. The improved compatibility between the PP and PET phases was also evident from the mechanical properties, as the compatibilized blend exhibited similar characteristics to the neat materials. Rheology measurements also demonstrate the ability of the compatibilizer to stabilize the blend and enhance its properties.

Furthermore, the mechanism underlying the compatibilization process was elucidated. FTIR-ATR, AFM-IR, and ^{1}H NMR measurements demonstrated that the compatibilizer's reactive glycidyl methacrylate functional groups underwent chemical reactions with the carboxyl groups of PET chains during processing. This resulted in significant enhancements in the overall morphology and fine-tuning of the mechanical and rheological properties of the material. In addition, it was possible to determine that the compatibilizer is at the interphase and, at higher concentrations, is also present in the dispersed phase.

Overall, this study provides valuable insights into using PTW as a compatibilizer for PP/PET blends. The optimized blend composition and the improved morphological and mechanical properties highlight the efficacy of PTW in enhancing the compatibility between these polymers. Understanding the underlying mechanism adds to the fundamental knowledge of compatibilization processes in polymer blends.

Author statement

Sebastián Coba-Daza: Data Curation, Formal analysis, Investigation, Writing - Original Draft.

Itziar Otaegi: Investigation, Writing - Review & Editing.

Nora Aramburu: Investigation, Writing - Review & Editing.

Gonzalo Guerrica-Echevarria: Writing - Review & Editing.

Lourdes Irusta: Investigation, Data Curation, Writing - Review & Editing.

Alba González: Investigation, Data Curation, Writing - Review & Editing.

Lena Neubauer: Investigation, Data Curation.

Georg Ramer: Investigation, Data Curation, Writing - Review & Editing.

Bernhard Lendl: Writing - Review & Editing.

Gerhard Hubner: Investigation, Data curation.

Dario Cavallo: Writing - Review & Editing, Funding acquisition, Supervision.

Davide Tranchida: Conceptualization, Writing - Review & Editing, Funding acquisition, Supervision.

Alejandro J Müller: Conceptualization, Writing - Review & Editing, Funding acquisition, Supervision.

Declaration of competing interest

We wish to confirm that there are no known conflicts of interest associated with this publication, and there has been no significant financial support for this work that could have influenced its outcome.

Data availability

Data will be made available on request.

Acknowledgements

This work has received funding from the European Union's Horizon 2020 research and innovation program under Grant Agreement No 860221 under the name of the REPOL project. The authors thank SGIker (UPV/EHU/ERDF, EU) for the technical and human support and the funding from the Basque Government through grant IT1503-22. The authors would also like to thank Walter Schaffer, Helmut Rinnerthaler, and Mahdi Abbasi from Borealis for sharing their expertise in polyolefin characterization. GR and BL acknowledge financial support through the COMET Centre CHASE, funded within the COMET Competence Centers for Excellent Technologies program by the BMK, the BMDW, and the Federal Provinces of Upper Austria and Vienna. The Austrian Research Promotion Agency (FFG) manages the COMET program. GR and LN acknowledge funding from the European Union's Horizon 2020 research and innovation program under Grant no. 953234 (Tumor-LN-oC), and GR acknowledges financial support under Grant no. 8619858 (PeroCUBE).

Appendix A. Supplementary data

Supplementary data to this article can be found online at https://doi.org/10.1016/j.polymertesting.2023.108293.

References

[1] Global plastic production and future trends | GRID-Arendal [Online]. Available: https://www.grida.no/resources/6923. (Accessed 14 March 2023).

[2] Martin, "UN projects world population to reach 8.5 billion by 2030, driven by growth in developing countries," United Nations Sustainable Development [Online]. Available: https://www.un.org/sustainabledevelopment/blog/2015/07/un-projects-world-population-to-reach-8-5-billion-by-2030-driven-by-growth-in-developing-countries/. (Accessed 14 March 2023).

[3] R. Geyer, J.R. Jambeck, K.L. Law, Production, use, and fate of all plastics ever made, Sci. Adv. 3 (7) (Jul. 2017), e1700782, https://doi.org/10.1126/sciadv.1700782.

[4] H. Jung, et al., Review of polymer technologies for improving the recycling and upcycling efficiency of plastic waste, Chemosphere 320 (Apr. 2023), 138089, https://doi.org/10.1016/j.chemosphere.2023.138089.

[5] X. Tang, et al., Upcycling of semicrystalline polymers by compatibilization: mechanism and location of compatibilizers, RSC Adv. 12 (18) (Apr. 2022) 10886–10894, https://doi.org/10.1039/D1RA09452A.

[6] N. C. Abdul Razak, A. H. Inuwa, and S. A. Samsudin, "Effects of compatibilizers on mechanical properties of PET/PP blend: Composite Interfaces: Vol 20, No 7," Compos. Interfac., vol. 20, no. 7, pp. 507–515, doi: https://doi.org/10.1080/15685543.2013.811176.

[7] A. Graziano, S. Jaffer, M. Sain, Review on modification strategies of polyethylene/polypropylene immiscible thermoplastic polymer blends for enhancing their mechanical behavior, J. Elastomers Plast. 51 (4) (Jun. 2019) 291–336, https://doi.org/10.1177/0095244318783806.

[8] M. Seier, V.-M. Archodoulaki, T. Koch, B. Duscher, M. Gahleitner, Polyethylene terephthalate based multilayer food packaging: deterioration effects during mechanical recycling, Food Packag. Shelf Life 33 (Sep. 2022), 100890, https://doi.org/10.1016/j.fpsl.2022.100890.

[9] C.P. Papadopoulou, N.K. Kalfoglou, Comparison of compatibilizer effectiveness for PET/PP blends: their mechanical, thermal and morphology characterization, Polymer 41 (7) (Mar. 2000) 2543–2555, https://doi.org/10.1016/S0032-3861(99)00442-5.

[10] R.A. Shanks, J. Li, L. Yu, Polypropylene–polyethylene blend morphology controlled by time–temperature–miscibility, Polymer 41 (6) (Mar. 2000) 2133–2139, https://doi.org/10.1016/S0032-3861(99)00399-7.

[11] S. Kordjazi, Z. Kordjazi, N. Golshan Ebrahimi, The effect of different compatibilisers on the morphology and rheological properties of PP/PET polymer blends, Plast., Rubber Compos. 51 (5) (May 2022) 250–258, https://doi.org/10.1080/14658011.2021.1981525.

[12] H.A. Khonakdar, S.H. Jafari, S. Mirzadeh, M.R. Kalaee, D. Zare, M.R. Saehb, Rheology-morphology correlation in PET/PP blends: influence of type of compatibilizer, J. Vinyl Addit. Technol. 19 (1) (Mar. 2013) 25–30, https://doi.org/10.1002/VNL.20318.

[13] Y.X. Pang, D.M. Jia, H.J. Hu, D.J. Hourston, M. Song, Effects of a compatibilizing agent on the morphology, interface and mechanical behaviour of polypropylene/poly(ethylene terephthalate) blends, Polymer 41 (1) (Jan. 2000) 357–365, https://doi.org/10.1016/S0032-3861(99)00123-8.

[14] M. Asgari, M. Masoomi, Thermal and impact study of PP/PET fibre composites compatibilized with Glycidyl Methacrylate and Maleic Anhydride, Composites, Part B 43 (3) (Apr. 2012) 1164–1170, https://doi.org/10.1016/j.compositesb.2011.11.035.

[15] N. Imamura, et al., Effectiveness of compatibilizer on mechanical properties of recycled PET blends with PE, PP, and PS, Mater. Sci. Appl. 5 (8) (Jun. 2014), https://doi.org/10.4236/msa.2014.58057. Art. no. 8.

[16] Y. Tao, K. Mai, Non-isothermal crystallization and melting behavior of compatibilized polypropylene/recycled poly(ethylene terephthalate) blends, Eur. Polym. J. 43 (8) (Aug. 2007) 3538–3549, https://doi.org/10.1016/j.eurpolymj.2007.05.007.

[17] I.M. Inuwa, A. Hassan, S.A. Samsudin, M.K.M. Haafiz, M. Jawaid, Interface modification of compatibilized polyethylene terephthalate/polypropylene blends:

effect of compatibilization on thermomechanical properties and thermal stability, J. Vinyl Addit. Technol. 23 (1) (2017) 45–54, https://doi.org/10.1002/vnl.21484.
[18] M. Ahmadlouydarab, M. Chamkouri, H. Chamkouri, Compatibilization of immiscible polymer blends (R-PET/PP) by adding PP-g-MA as compatibilizer: analysis of phase morphology and mechanical properties, Polym. Bull. 77 (11) (Nov. 2020) 5753–5766, https://doi.org/10.1007/s00289-019-03054-w.
[19] M. Entezam, et al., Influence of interfacial activity and micelle formation on rheological behavior and microstructure of reactively compatibilized PP/PET blends, Macromol. Mater. Eng. 297 (4) (2012) 312–328, https://doi.org/10.1002/mame.201100121.
[20] A. Ekinci, M. Öksüz, M. Ates, I. Aydin, Polypropylene/postconsumer recycled poly (ethylene terephthalate) hybrid composites: evaluation of morphological, mechanical, thermal and electrical properties, Iran. Polym. J. (Engl. Ed.) 31 (10) (Oct. 2022) 1283–1295, https://doi.org/10.1007/s13726-022-01076-2.
[21] M. Kaci, A. Benhamida, S. Cimmino, C. Silvestre, C. Carfagna, Waste and virgin LDPE/PET blends compatibilized with an ethylene-butyl acrylate-glycidyl methacrylate (EBAGMA) terpolymer, 1, Macromol. Mater. Eng. 290 (10) (2005) 987–995, https://doi.org/10.1002/mame.200500217.
[22] K. Van Kets, L. Delva, K. Ragaert, Structural stabilizing effect of SEBSgMAH on a PP-PET blend for multiple mechanical recycling, Polym. Degrad. Stabil. 166 (Aug. 2019) 60–72, https://doi.org/10.1016/j.polymdegradstab.2019.05.012.
[23] L.M.G. Araujo, A.R. Morales, Compatibilization of recycled polypropylene and recycled poly (ethylene terephthalate) blends with SEBS-g-MA, Polímeros 28 (Mar. 2018) 84–91, https://doi.org/10.1590/0104-1428.03016.
[24] J.-K. Kim, C.-H. Kim, M.-H. Park, Effects of multiple recycling on the structure and morphology of SEBS/PP composites, Bull. Kor. Chem. Soc. 37 (6) (2016) 820–825, https://doi.org/10.1002/bkcs.10776.
[25] Á.A. Matias, et al., Use of recycled polypropylene/poly(ethylene terephthalate) blends to manufacture water pipes: an industrial scale study, Waste Manag. 101 (Jan. 2020) 250–258, https://doi.org/10.1016/j.wasman.2019.10.001.
[26] Z.O.G.G. Schyns, M.P. Shaver, Mechanical recycling of packaging plastics: a Review, Macromol. Rapid Commun. 42 (3) (Feb. 2021), 2000415, https://doi.org/10.1002/MARC.202000415.
[27] D. Kurouski, A. Dazzi, R. Zenobi, A. Centrone, Infrared and Raman chemical imaging and spectroscopy at the nanoscale, Chem. Soc. Rev. 49 (11) (Jun. 2020) 3315–3347, https://doi.org/10.1039/C8CS00916C.
[28] A. Dazzi, C.B. Prater, AFM-IR: technology and applications in nanoscale infrared spectroscopy and chemical imaging, Chem. Rev. 117 (7) (Apr. 2017) 5146–5173, https://doi.org/10.1021/acs.chemrev.6b00448.
[29] A.C.V.D. dos Santos, B. Lendl, G. Ramer, Systematic analysis and nanoscale chemical imaging of polymers using photothermal-induced resonance (AFM-IR) infrared spectroscopy, Polym. Test. 106 (Feb. 2022), 107443, https://doi.org/10.1016/j.polymertesting.2021.107443.
[30] A.C.V.D. dos Santos, D. Tranchida, B. Lendl, G. Ramer, Nanoscale chemical characterization of a post-consumer recycled polyolefin blend using tapping mode AFM-IR, Analyst 147 (16) (Aug. 2022) 3741–3747, https://doi.org/10.1039/D2AN00823H.
[31] H. Inata, S. Matsumura, Chain extenders for polyesters. I. Addition-type chain extenders reactive with carboxyl end groups of polyesters, J. Appl. Polym. Sci. 30 (8) (1985) 3325–3337, https://doi.org/10.1002/app.1985.070300815.
[32] L. Hu, P.Y. Vuillaume, Chapter 7 - reactive compatibilization of polymer blends by coupling agents and interchange catalysts, in: A. A.r, S. Thomas (Eds.), Compatibilization of Polymer Blends, Elsevier, 2020, pp. 205–248, https://doi.org/10.1016/B978-0-12-816006-0.00007-4.
[33] P. Raffa, M.-B. Coltelli, V. Castelvetro, Expanding the application field of post-consumer poly(ethylene terephthalate) through structural modification by reactive blending, J. Appl. Polym. Sci. 131 (19) (2014), https://doi.org/10.1002/app.40881.
[34] C. Huang, et al., Design of super-toughened, heat-resistant and antistatic polyethylene terephthalate-based blend composites by constructing a tenacious interface, Polymer 277 (Jun. 2023), 125966, https://doi.org/10.1016/j.polymer.2023.125966.
[35] M. Akbari, A. Zadhoush, M. Haghighat, PET/PP blending by using PP-g-MA synthesized by solid phase, J. Appl. Polym. Sci. 104 (6) (Jun. 2007) 3986–3993, https://doi.org/10.1002/APP.26253.
[36] Sabu Thomas, A. A. R, Compatibilization of Polymer Blends : Micro and Nano Scale Phase Morphologies, Interphase Characterization and Properties, Elsevier, San Diego, 2019 [Online]. Available: https://public.ebookcentral.proquest.com/choice/publicfullrecord.aspx?p=5942009.
[37] Domasius Nwabunma, T. Kyu, Polyolefin blends, in: Wiley Series on Polymer Engineering and Technology, Wiley-Interscience, Hoboken, N.J., 2008, https://doi.org/10.1002/9780470199008.
[38] A. Ghosh, Performance modifying techniques for recycled thermoplastics, Resour. Conserv. Recycl. 175 (Dec. 2021), 105887, https://doi.org/10.1016/j.resconrec.2021.105887.
[39] C. Koster, V. Altstädt, H.H. Kausch, W.J. Cantwell, Split rate fatigue propagation in polymer blends, Polym. Bull. 34 (2) (Feb. 1995) 243–248, https://doi.org/10.1007/BF00316402.
[40] R. Bahrami, T.I. Löbling, H. Schmalz, A.H.E. Müller, V. Altstädt, Synergistic effects of Janus particles and triblock terpolymers on toughness of immiscible polymer blends, Polymer 109 (Jan. 2017) 229–237, https://doi.org/10.1016/j.polymer.2016.12.044.
[41] Z. Bartczak and A. Galeski, Mechanical Properties of Polymer Blends, Second. SpringerLink. [Online]. Available: https://doi.org/10.1007/978-94-007-6064-6_13.
[42] H. Kang, X. Lu, Y. Xu, Properties of immiscible and ethylene-butyl acrylate-glycidyl methacrylate terpolymer compatibilized poly (lactic acid) and polypropylene blends, Polym. Test. 43 (May 2015) 173–181, https://doi.org/10.1016/j.polymertesting.2015.03.012.
[43] Z. Kordjazi, N.G. Ebrahimi, Rheological behavior of noncompatibilized and compatibilized PP/PET blends with SEBS-g-MA, J. Appl. Polym. Sci. 116 (1) (2010) 441–448, https://doi.org/10.1002/app.31471.
[44] N. Zdrazilova, B. Hausnerova, T. Kitano, P. Saha, Rheological behaviour of PP/PET and modified PP/PET blends. I. Steady state flow properties, Polym. Polym. Compos. 11 (6) (Sep. 2003) 487–503, https://doi.org/10.1177/096739110301100607.
[45] J.-C. Lepers, B.D. Favis, C. Lacroix, The influence of partial emulsification on coalescence suppression and interfacial tension reduction in PP/PET blends, J. Polym. Sci., Part B: Polym. Phys. 37 (9) (1999) 939–951, https://doi.org/10.1002/(SICI)1099-0488(19990501)37:9<939::AID-POLB6>3.0.CO;2-O.